

Molecular Iodine-Catalyzed Synthesis of Imidazo[1,2-*a*]Pyridines: Screening of Their *In Silico* Selectivity, Binding Affinity to Biological Targets, and Density Functional Theory Studies Insight

Deepika Geedkar, Ashok Kumar, and Pratibha Sharma*

Cite This: *ACS Omega* 2022, 7, 22421–22439

Read Online

ACCESS |



Metrics & More

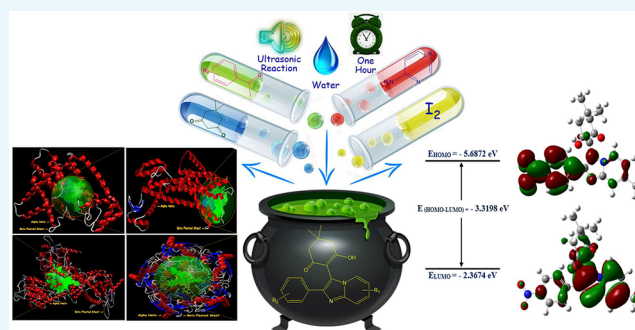


Article Recommendations



Supporting Information

ABSTRACT: The present paper discloses an ultrasonication strategy assisted by molecular iodine as an environmentally benign catalyst leading to the synthesis of pharmacologically significant imidazo[1,2-*a*]pyridine scaffolds. The molecular-iodine-catalyzed approach for the synthesis of biologically active synthetic equivalents was achieved through three-component coupling embracing 2-aminopyridine derivatives, pertinent acetophenones, and dimedone in water medium under aerobic conditions. The higher product yield (up to 96%) with a miniature reaction time and modest catalyst loading as demonstrated by higher ecological compatibility and sustainability factors are fascinating features of this protocol. The structures of synthesized compounds were accomplished through FT-IR, ¹H NMR, ¹³C NMR, mass, and elemental analysis data. The virtual screening of synthetic moieties was performed to ascertain the *in silico* selectivity and binding affinities against several biological targets. Lipinski's rules of five, ADMET, and TOPKAT descriptors were used to evaluate the drug-likeness assets. Furthermore, a quantum computational study was computed at the B3LYP/6-311G++(d,p) level of theory to investigate the density functional theory-based chemical reactivity parameters and HOMO–LUMO energy gap of the synthesized derivatives. The present studies open the way for *in vitro* and *in vivo* testing of synthesized derivatives as potent inhibitors with an improved pharmacological profile against farnesyl diphosphate synthase, phosphodiesterase III, CXCR4, and GABA_A receptor agonists.



1. INTRODUCTION

Multicomponent reactions (MCRs) have been cherished in the realm of structural diversity and complexity in organic synthesis provisioning access to diverse sets of heterocyclic motifs.¹ In a particular context, the imidazo-fused pyridines are one of the fascinating classes of nitrogen-fused heterocyclic scaffolds of versatile concern. Their chemistry has drawn significant attention over the past few years owing to their endowment in diverse medicinal applications, *viz.*, antiviral, anticancer, anti-inflammatory, antibacterial, and anxiolytic agents.²

Furthermore, several drugs embracing the imidazo-fused pyridine skeleton have been commercially marketed with their trade names as minodronic acid, a farnesyl diphosphate synthase inhibitor for the treatment of osteoporosis,³ olprinone,⁴ a phosphodiesterase III inhibitor as a cardiotoxic agent for acute heart failure, zolpidem,⁵ a benzodiazepine γ -aminobutyric acid (GABA) receptor agonist for insomnia, zolimidine,⁶ for the treatment of peptic ulcers, alpidem, saripidem, and necopidem,^{5,7} a GABA_A receptor agonist used as an anxiolytic agent, and some are under development, like GSK812397, a chemokine receptor, CXCR4 antagonist for the treatment of HIV,⁸ and β -amyloid formation inhibitors for Alzheimer's disease^{5,7} as depicted in Figure 1. Further, the imidazo[1,2-*a*]pyridine

derivatives have also been utilized as abnormal N-heterocyclic carbene ligands and have some noteworthy applications in material sciences and agrochemicals.^{9,10}

Over the past decades, the synthesis of fused bicyclic imidazo[1,2-*a*]pyridines has elicited much consideration and resulted in the development of a variety of synthetic methodologies.¹¹ In recent times, a number of multicomponent syntheses of imidazo[1,2-*a*]pyridines have been reported embracing assistance of a number of catalysts, *viz.*, Cu(OTf)₂, CuI/Cu(OTf)₂, ionic liquid BPyBF₄, FeCl₂, FeCl₃, Sc(OTf)₃, ZrCl₂, montmorillonite clay, InCl₃, bromodimethyl sulfonium bromide (BDMS), copper(I) iodide-NaHSO₄·SiO₂, magnetic nano-Fe₃O₄-KHSO₄·SiO₂, CeCl₃·7H₂O/NaI, and dichloro(2-pyridinecarboxylato) gold [PicAuCl₂].¹¹ However, these methods endure some bottlenecks including the requirement of expensive and excessive amounts of catalysts, harsh reaction

Received: March 16, 2022

Accepted: June 1, 2022

Published: June 22, 2022



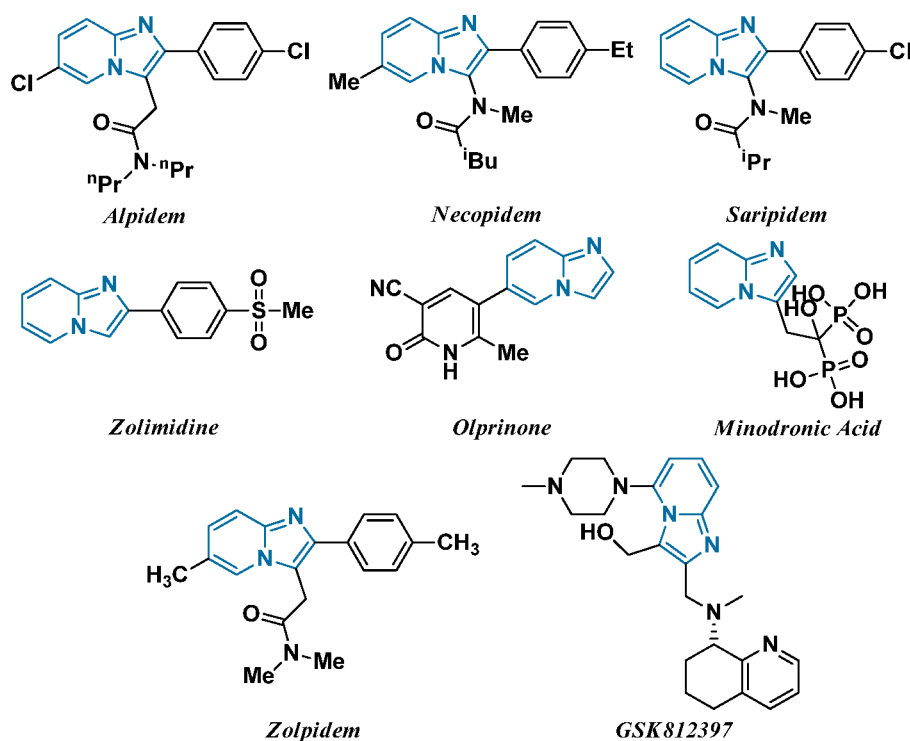
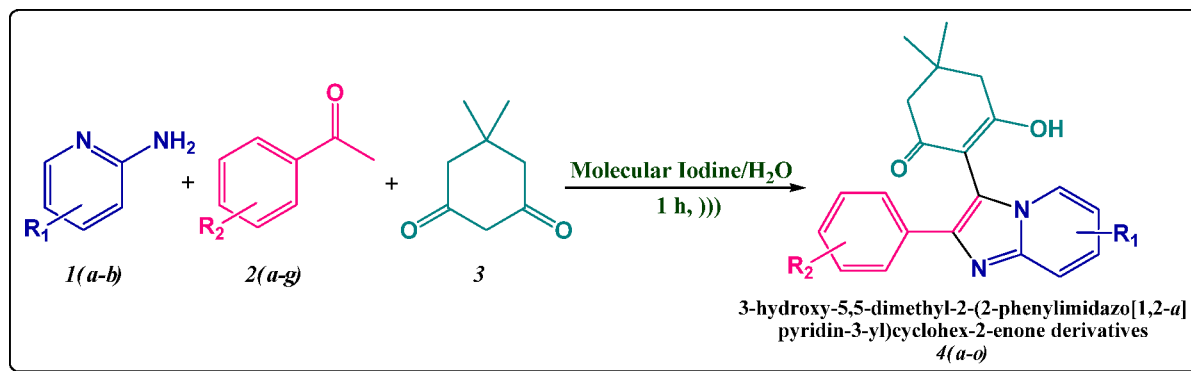


Figure 1. Some representative biologically active drugs embraced with an imidazole-fused pyridine skeleton.

Scheme 1. Ultrasonic-Assisted Synthesis of 2-Phenylimidazo[1,2-*a*]pyridin-3-yl Derivatives 4(a-o)



conditions, product diversity, and yields. Hence, keeping this in view, it was thought to be worthwhile to develop a simple and high-yielding environmentally benign protocol for the one-pot multicomponent synthesis of fused bicyclic imidazo[1,2-*a*]pyridine scaffolds.

Most organic reactions, including multicomponent transformations, use dimedone or its derivatives as a versatile synthon. The acidic feature of dimedone's methylene group, which is in equilibrium with the tautomeric enol form, is responsible for its notoriety. These findings support the use of dimedone in a variety of organic processes that result in a variety of organic compounds with high medicinal potency. Their versatile chemistry with its low toxicity, easy accessibility and handling, moisture stability, and low cost make them pertinent precursors for the production of divergent organic compounds possessing anticancer, antioxidant, spasmolytic, anti-anaphylactic, and antibacterial activities. They have also emerged as a substantial class of compounds owing to their industrial and synthetic applications including several uses in dyes, fluorescent compounds, and laser technology. The organic transformations

are performing on the basis of green chemistry procedures that are in demand over the last few decades.¹²

Because of accruing concerns over a hazardous sequel of organic solvents for the environment and living creatures, diverse types of MCRs have been effectively investigated in the aqueous medium. The reactions in an aqueous environment have spurred interest owing to its elite reactivity and selectivity that are onerous to acquire in conventional organic solvents. Water, probably because of its unique abilities, for instance, hydrogen bonding, high dielectric constant, and polarity, appears to be a more rational medium for organic transformation. In this framework, water is a preferential solvent providing an astonishing contribution to the field of organic synthesis.¹³

During recent decades, iodine has been evinced to be a versatile and benign reagent in the synthesis of a wide range of heterocyclic moieties including benzimidazoles,¹⁴ benzoxazoles, benzothiazole,¹⁵ quinolines,¹⁶ coumarins,¹⁷ and lactones.¹⁸ Molecular iodine has received escalating significance owing to its low outlay, nontoxicity, sustainability, ready availability, and

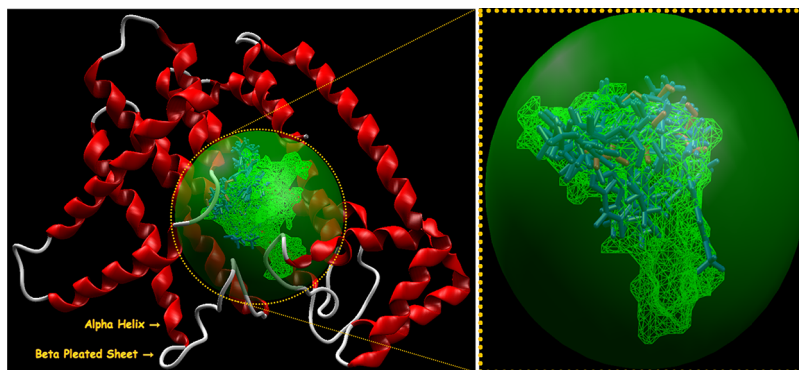


Figure 2. Secondary structure of farnesyl diphosphate synthase binds with imidazo[1,2-*a*]pyridin-3-yl derivatives **4(a-o)** (blue) and standard drug minodronic acid (pink) inside the cavity (green framework).

ecofriendly properties as the preferable catalyst for organic synthesis. The utilization of iodine as a Lewis acid has improved substantially on account of its high tolerance to air as well as moisture and high catalytic activity in dilute and highly concentrated conditions.^{19,20}

Computational approaches have become essential complements to each stage of the drug discovery and development trajectory. Molecular docking is an emphatic strategy to gain insight into the interactions between ligand and receptor in the design and development of the drug candidates. The significant role of molecular docking in the development of drug design is because of its ability to predict the best binding mode between drugs and the target protein. However, the density functional theory (DFT) method has also emerged as an influential technique for appraising the structural and spectral properties of organic compounds. The global and local chemical reactivity parameters and the impact of pertinent substituted groups on the synthesized scaffold were also achieved by utilizing the DFT method.²¹

Hence, encouraged by these advances, we sought to explore the relevance of these reagents and methods in the synthesis of fused imidazo-pyridine scaffolds. In continuation of our research program focused on the development of synthetic methodologies^{22–24} herein, we wish to disclose for the first time the ultrasonic-assisted synthesis of 2-phenylimidazo[1,2-*a*]pyridin-3-yl cyclohex-2-enones derivatives by employing iodine as a catalyst in aquatic conditions via one-pot MCR of 2-amino-pyridine derivatives and pertinent aryl aldehydes along with dimedone embracing differently as one of the precursor substrates (Scheme 1). To the best of our knowledge, the use of dimedone as a precursor for the synthesis of imidazo[1,2-*a*]pyridine scaffolds by utilizing molecular iodine is hitherto unprecedented.

2. EXPERIMENTAL SECTION

2.1. General Procedure for the Ultrasonic-Assisted Synthesis of 2-Phenylimidazo[1,2-*a*]pyridin-3-yl Derivatives **4(a-o).** A mixture of acetophenone derivatives **2(a-g)** (1.0 mmol) and a catalytic amount of (20 mol %) iodine in 4.0 mL of distilled water was irradiated utilizing an ultrasound at room temperature for 30 min. Then, 2-aminopyridine derivatives **1(a-b)** (1.0 mmol) and dimedone (**3**) (1.0 mmol) were added to the above mixture and again irradiated, employing ultrasound at room temperature for the ambient time (30 min). As the reaction time is very short, there was not a substantial elevation of temperature due to ultrasonic shock. The ultrasonic apparatus

used showed the temperature automatically, so the temperature was controlled and fixed at room temperature by a water circulator in the case of any elevation of temperature.^{22–24} The progress of the reaction was monitored through TLC (on aluminum sheets precoated with silica) using *n*-hexane/ethyl acetate (4:1) as the eluting system. After the completion of the reaction, 15.0 mL of 10 mol % sodium thiosulfate solution was added and extracted with ethyl acetate (3 × 20 mL). The organic layer was dried over anhydrous Na₂SO₄ and concentrated under a vacuum. The crude product was filtered off and purified by recrystallization from methanol to afford the pure products **4(a-o)** (Scheme 1).

The analytical and spectroscopic data for each of the synthesized derivatives **4(a-o)** are summarized in Supporting Information.

2.2. Preparation of Protein and Ligand for Docking Study. The X-ray crystallographic structures of the human farnesyl diphosphate synthase (PDB ID: 5CG5),²⁵ human phosphodiesterase 3B (PDB ID: 1SO2),²⁶ human GABAA (PDB ID: 4COF),²⁷ and CXCR4 (PDB ID: 3OE0)²⁸ with a resolution of 1.40, 2.40, 2.97, and 2.90 Å, respectively, have been retrieved from the Research Collaboratory for Structural Bioinformatics–Protein Data Bank (RCSB–PDB). The imidazo[1,2-*a*]pyridin-3-yl derivatives **4(a-o)** were screened against human farnesyl diphosphate synthase, human phosphodiesterase 3B, human GABAA, and CXCR4 targets for the prediction of selectivity and binding affinity.

The Molegro Virtual Docker (MVD 2013.6.0.0 evaluation version)²⁹ was used for performing docking studies, which are based on molecular docking (MD) simulations *viz.* ligand and macromolecular interaction energy. The docking score function (E_{score}) is described by the following energy terms,

$$E_{\text{score}} = E_{\text{inter}} + E_{\text{intra}}$$

where E_{inter} is the ligand-protein interaction energy, E_{intra} is the internal energy of the ligand

$$E_{\text{inter}} = \sum_{i \in \text{ligand}} \sum_{j \in \text{protein}} \left(E_{\text{PLP}}(r_{ij}) + 332.0 \frac{q_i q_j}{4r_{ij}^2} \right)$$

The summation considers all heavy atoms of the ligand and protein, wherein the cofactor atoms and water molecules have been taken into consideration if present, whereas the electrostatic interactions between charged atoms are considered by the second term.

$$E_{\text{intra}} = \sum_{i \in \text{ligand}} \sum_{j \in \text{protein}} E_{\text{PLP}}(r_{ij}) + \sum_{\text{flexible bonds}} A [1 - \cos(m \times \theta - \theta_0) + E_{\text{clash}}]$$

First, the geometrically optimized three-dimensional structures of imidazo[1,2-*a*]pyridin-3-yl derivatives **4(a-o)** were imported into the workspace of MVD accompanied by the individual target structure, retrieved from the RCSB Protein Data Bank for performing the molecular docking simulations. The geometrical optimizations of imidazo[1,2-*a*]pyridin-3-yl derivatives **4(a-o)** were procured by performing the molecular mechanics (MM2) and Hamiltonian approximation (AM1) optimizers until the root-mean-square (RMS) gradient value attains a value smaller than 0.001 kcal mol⁻¹ Å⁻¹. While the target protein was imported, all of the crystallographic water molecules were detached from it. Further, all the ligands and targets were refined with the protein preparation wizard extant at the preparation window in the workspace of MVD, followed by the identification and detection of active sites (cavities) within the target protein.

During this computational process, the maximum numbers of cavities were set to five, the grid resolution to 0.80 Å, and the probe size to 1.2 Å, while the other parameters were taken as default.³⁰ The docking scores indicate the significant binding interactions, i.e., hydrogen-bonding and steric interactions that take place between the ligand of different conformations and key amino acid residues in the binding pocket of the target. Furthermore, the Mol Dock score is the sum of internal ligand energies, protein interaction energies, and soft penalties. The protein–ligand energy is the total interaction energy between the ligand and the target molecule, whereas the steric score indicates the interaction energy between the ligand and protein. The H-bond score is the hydrogen-bonding energy between the protein and ligand. The reranking score function is computationally more valuable than the scoring function used during the docking simulations. In general, the rerank score is better than the docking score function for determining the best pose among the various poses derived from the identical ligand.^{30,31}

The active sites or cavities (1–5) with diverse surface areas and volumes within the selected targets for screening are depicted in Table S5 of the Supporting Information using the detect cavity module in MVD.³¹ The secondary structures of the selected targets with detected active sites (1–5) were visualized using Molegro Virtual Docker²⁹ and are presented in Figure 1S of the Supporting Information. The MD simulations were performed within the cavity of the larger surface area of protein. Some other parameters such as binding radius, grid resolution, and maximum iteration parameters were set to 15 Å, 0.3 Å, and 1500, respectively. The docking algorithm was set to MolDock Simplex Evolution (MolDock SE) docking algorithm with a population size of 50. For cluster similar poses and ignore similar poses (for multiple runs only), the RMSD thresholds were firm to 1.00 Å. The number of independent runs was retained as 10, and each of these runs was recurred to a single final solution (Pose). After the completion of docking simulations, only the negative lowest-energy representative cluster was returned from each of them, followed by the removal of all the similar poses and keeping the best scoring pose. The clusters were ranked in order of increasing the lowest binding energy conformation in each cluster. The analyses of the molecular docking results were performed on the first binding free energy pose with minimum energy.^{30,31} The secondary structures of the selected targets bind with imidazo[1,2-*a*]pyridin-3-yl derivatives **4(a-o)** (blue) and

standard drugs (pink) inside the cavities (green framework) envisaged by Molegro Virtual Docker (MVD 2013.6.0.0 evaluation version)²⁸ and illustrated in Figures 2, 4, 6, and 8, respectively.

2.3. Prediction of ADMET, Toxicity, and Drug-Likeness Properties. The drug-likeness of all of the synthesized compounds **4(a-o)** and standard drugs were evaluated by assessing Lipinski's rules, absorption, distribution, metabolism, excretion, and toxicity (ADMET) descriptors, and TOPKAT descriptors utilizing Accelrys Discovery studio package.³² The ADMET analyses were achieved using some descriptors, for instance, absorption, solubility, atom-based Log P98 (ALogP98), ADME 2D polar surface area (ADME 2D PSA), blood–brain barrier (BBB), cytochrome P4502D6 (CYP2D6), and hepatotoxicity (HEPATOX), and plasma protein binding (PPB). Furthermore, the Toxicity Prediction by Computer-Assisted Technology (TOPKAT) analyses were attained using carcinogenic potency of the National Toxicology Program (NTP) Carcinogenicity of Male Rat and Mouse, Ames Mutagenicity, Skin Irritancy, Aerobic Biodegradability.³³

2.4. DFT-Based Chemical Reactivity Parameters. All the molecular structures of imidazo[1,2-*a*]pyridin-3-yl derivatives **4(a-o)** were optimized at the B3LYP level of theory using the 6-311G++(d,p) basis set of the Gaussian 09 program suite.³⁴ The global chemical reactivity parameters consist of total energy, electrophilicity (ω), chemical hardness (η), and electronic chemical potential (μ). The stability and reactivity of the molecules are appraised by these parameters.³⁵ The calculated results were obtained using the HOMO and LUMO energies according to Koopmans' theorem and Parr approximation.^{36,50}

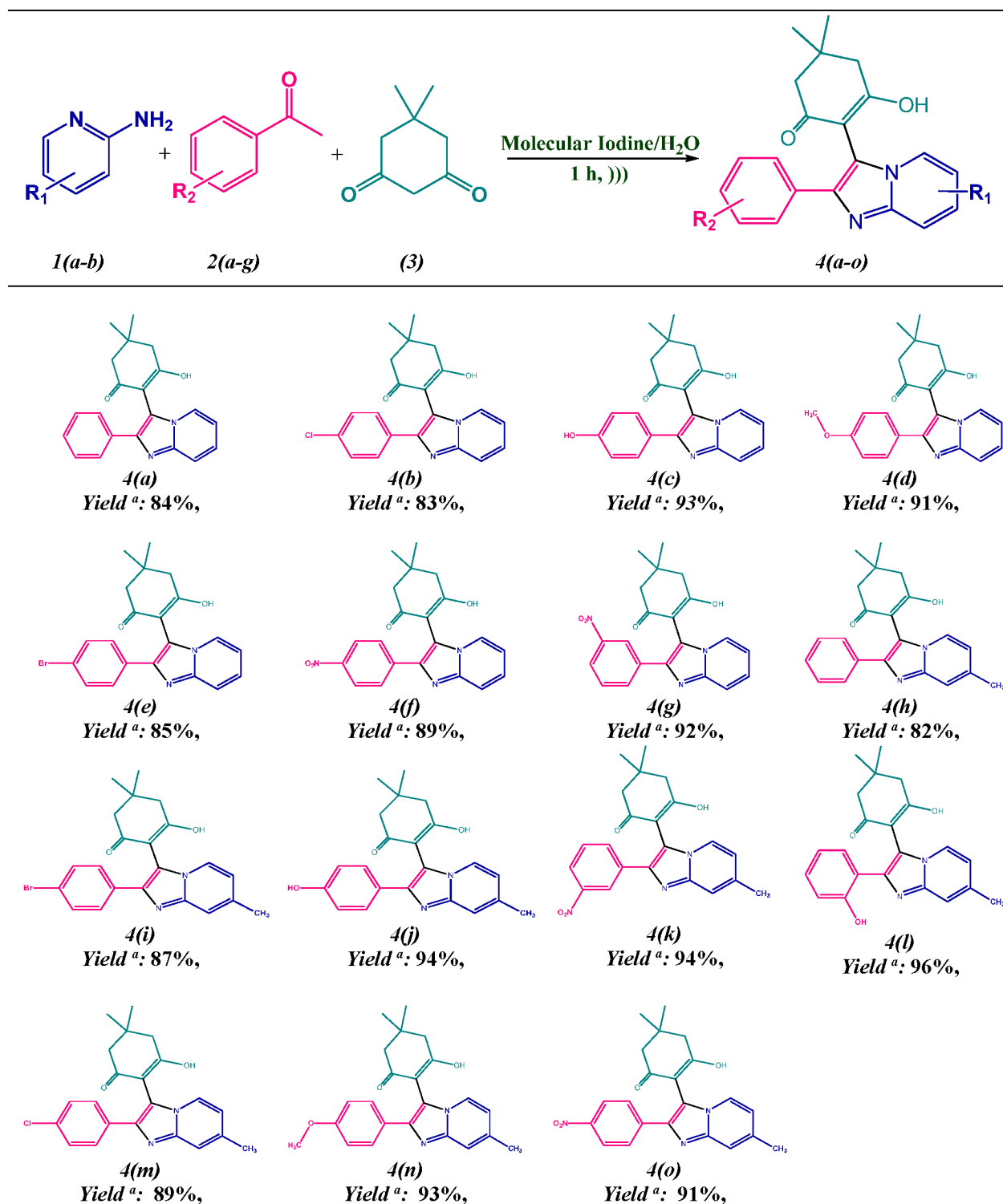
$$\eta = \frac{E_{\text{HOMO}} - E_{\text{LUMO}}}{2}$$

The HOMO–LUMO energy gap is used for assessing the chemical hardness as well as for determining the stability of the molecular structure.³⁶ It is recognized that the higher the HOMO–LUMO energy gap, the more stable and chemically harder the molecules in contrast to the softer and less stable molecules. The parameter electrophilicity index (ω) is delineated as the lowering in energy of molecules due to the flow of electrons from the highest occupied molecular orbital to the lowest unoccupied molecular orbital. Hence, it measures the

Table 1. Optimization of Reaction Conditions for the Sonochemical Synthesis of 3-Hydroxy-5,5-dimethyl-2-(2-phenylimidazo[1,2-*a*]pyridin-3-yl)cyclohex-2-enone **4(a)^a**

entry	source of iodine	solvent	time (h) ^b	yield ^c
1	–	–	2	NR
2	–	H ₂ O	2	NR
3	NaI	H ₂ O	1	28
4	KI	H ₂ O	1	33
5	CuI	H ₂ O	1	55
6	ZnI ₂	H ₂ O	1	47
7	I ₂ (15 mol %)	–	1.5	62
8	I ₂ (15 mol %)	H ₂ O	1	79
9	I ₂ (20 mol %)	H ₂ O	1	84
10	I ₂ (20 mol %)	H ₂ O	1.5	84
11	I ₂ (25 mol %)	H ₂ O	1	83

^aReaction conditions: 2-aminopyridine (1 mmol) **1(a)**, acetophenone (1 mmol) **2(a)**, and dimedone (1 mmol) (**3**). ^bAll the reactions were monitored by TLC. ^cIsolated yield.

Table 2. Substrate Scope for the Ultrasonic-Assisted Synthesis of 2-Phenylimidazo[1,2-*a*]pyridin-3-yl)cyclohex-2-enones Derivatives 4(a-o)^a

^aReaction conditions: 2-aminopyridine derivatives (1 mmol) 1(a-b), pertinent acetophenone (1 mmol) 2(a-g), dimedone (1 mmol) (3), and a catalytic amount (20 mol %) of I₂ was irradiated for 1 h in the presence of water. Reactants 2(a-g) and (3) were added to the reaction mixture only after the disappearance of the reactant 1(a-b). ^bIsolated yield.

energy changes that take place when a molecule is saturated by the addition of electrons and governs the chemical reactivity behavior of the molecules.^{37,38} The following equation represents the electrophilicity index (ω) of molecules as follows,

$$\omega = \frac{\mu^2}{2\eta}$$

Electronic chemical potential (μ) is described as the negative of electronegativity and is given by the equation as³⁶

Scheme 2. Plausible Mechanistic Pathway for the Synthesis of 2-Phenylimidazo[1,2-*a*]pyridin-3-yl)cyclohex-2-enones Scaffolds 4(a-o)

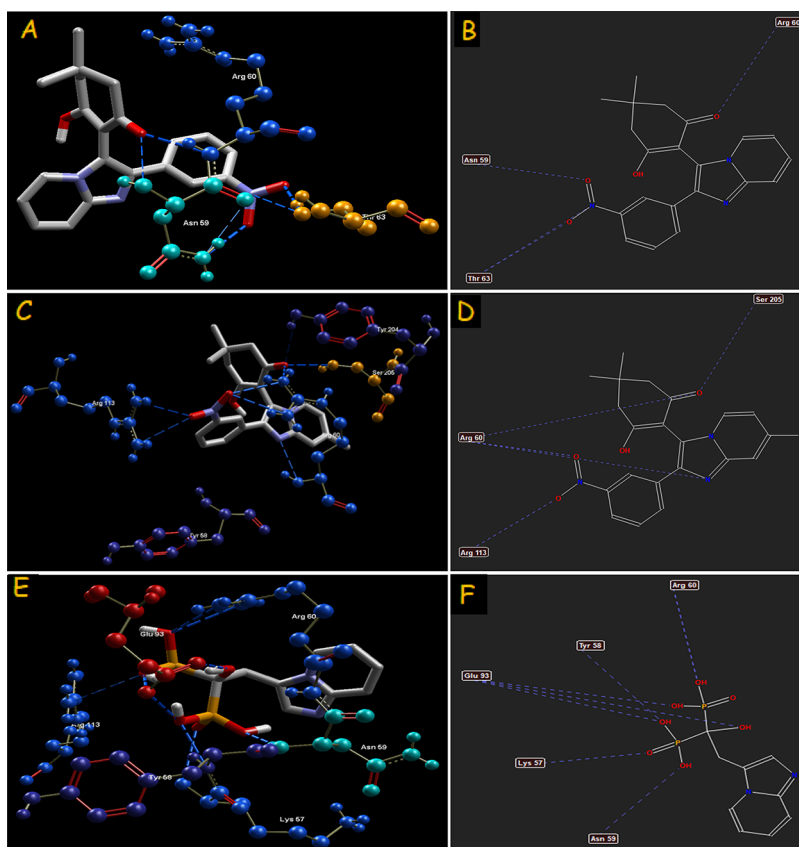
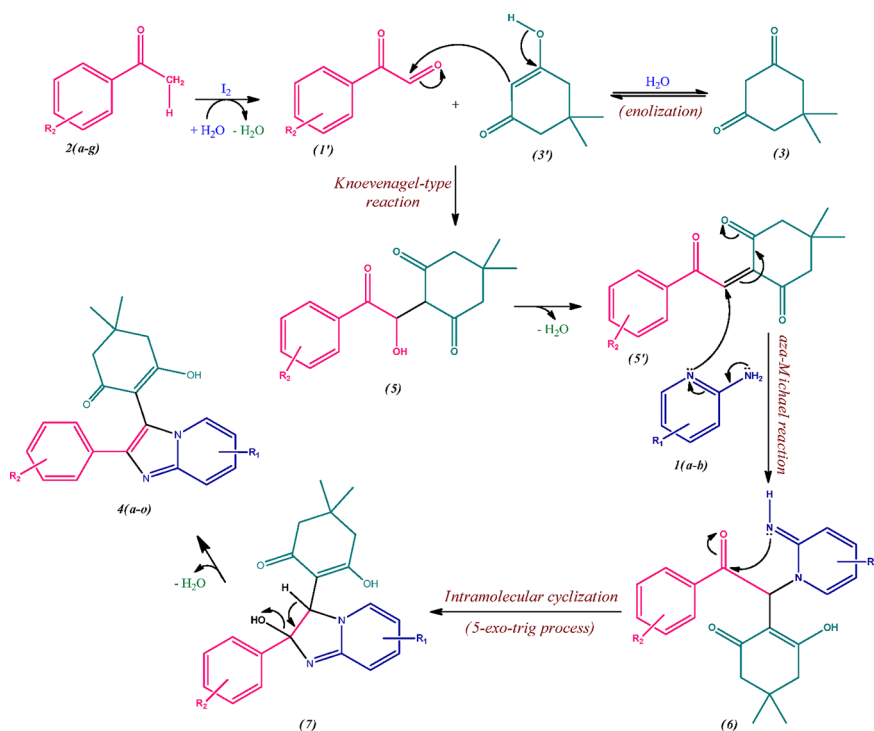


Figure 3. Hydrogen-bond interaction of compounds 4(k) (A–B), 4(g) (C–D), and standard drug minodronic acid (E–F) with farnesyl diphosphate synthase target.

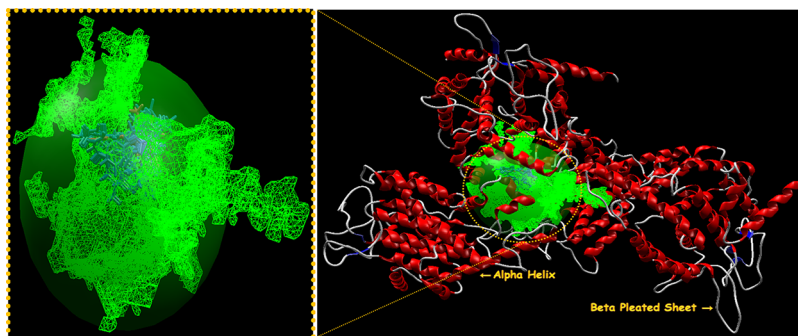


Figure 4. Secondary structure of phosphodiesterase 3B binds with imidazo[1,2-*a*]pyridin-3-yl derivatives 4(a-o) (blue) and standard drug olprinone (pink) inside the cavity (green framework).

Table 3. Docking Scores^a of Imidazo[1,2-*a*]pyridin-3-yl Derivatives 4(a-o) Docked with Farnesyl Diphosphate Synthase Target Selected for Screening

compound name	MolDock score	rerank score (kJ/mol)	interaction energy (kJ/mol)	steric	HBond (kJ/mol)
4(a)	-121.070	-46.2331	-129.523	-125.412	-4.12665
4(b)	-116.882	-86.3746	-127.038	-123.787	-3.25102
4(c)	-119.894	-92.4212	-131.989	-126.252	-5.73747
4(d)	-121.378	-92.2706	-133.879	-130.228	-3.65058
4(e)	-116.694	-86.3413	-126.942	-123.758	-3.18489
4(f)	-124.997	-82.7741	-139.449	-130.422	-11.7324
4(g)	-136.382	-97.9987	-148.481	-139.207	-9.27341
4(h)	-121.380	-91.9035	-131.591	-129.897	-5.74383
4(i)	-115.326	-78.1772	-126.461	-119.791	-6.66971
4(j)	-123.665	-94.6358	-134.444	-128.501	-5.94368
4(k)	-145.600	-107.580	-149.188	-136.328	-12.8601
4(l)	-126.914	-97.9745	-138.142	-133.722	-8.41212
4(m)	-117.557	-89.4801	-128.437	-124.994	-3.44365
4(n)	-125.239	-94.7880	-136.104	-132.444	-3.65975
4(o)	-125.450	-87.6107	-135.379	-124.855	-10.5236
minodronic acid	-111.023	-88.7053	-117.088	-97.5360	-19.5515

^aMolDock score, rerank score, protein–ligand interaction, H-bond, and steric score.

$$\mu = \frac{E_{\text{HOMO}} + E_{\text{LUMO}}}{2}$$

where η represents chemical hardness, ω represents electrophilicity index of molecules, and μ represents the electronic chemical potential.

It depicts the transfer of charge that takes place within the molecule in the ground state which describes the tendency of electrons to escape from the equilibrium state. Hence, chemically reactive molecules show a greater chemical potential.

The condensed Fukui functions (FF) were utilized to rationalize and predict the reactivity profile of the molecule, which were evaluated on the basis of atomic charges obtained from electron density population analysis using the following equations,³⁹

$$\text{Nucleophilic attack: } f_k^+ = qk(N+1) - qk(N)$$

$$\text{Electrophilic attack: } f_k^- = qk(N) - qk(N-1)$$

$$\text{Radical attack: } f_k^0 = (qk(N+1) - qk(N-1)) / 2$$

where $qk(N)$ is the charge on the atom k for (N) total electrons, $qk(N+1)$ is the charge on the atom k for $(N+1)$ total electrons, $qk(N-1)$ is the charge on the atom k for $(N-1)$ total electrons, respectively.

Here, the highest positive values of the Fukui function indicate the most probable atomic sites for the nucleophilic (f_k^+), electrophilic (f_k^-), and radical attacks (f_k^0).⁴⁰

2.5. Data and Software Availability. The X-ray crystallographic structures of the biological targets were retrieved from the Research Collaboratory for Structural Bioinformatics–Protein Data Bank (RCSB–PDB). All of the chemical structures were produced from ChemDraw Ultra 11.0. The docking studies were performed adopting the Molegro Virtual Docker (MVD 2013.6.0.0 evaluation version). All of the quantum computational studies were computed at the B3LYP level of theory using the 6-31G++(d,p) basis set of the Gaussian 09 program suite. The drug-likeness properties were analyzed by assessing Lipinski's rules, absorption, distribution, metabolism, excretion, and toxicity (ADMET) descriptors, and TOPKAT descriptors utilizing the Accelrys Biovia Discovery Studio 2019 package. The full workflow is reported in the Experimental Section.

3. RESULTS AND DISCUSSION

3.1. Optimization of Reaction Conditions. We have developed a green and efficient methodology for the preparation of tetrasubstituted imidazole-fused pyridine tethered with dimedone via readily available reactants. We envisaged that the synthesis of our desired products was attained from the condensation reaction of phenylglyoxal derivatives, pertinent 2-aminopyridines, and dimedone. After considering the expenses

Table 4. Molecular Interactions Analyses of Imidazo[1,2-*a*]pyridin-3-yl Derivatives 4(a-o) and Standard Drug with Farnesyl Diphosphate Synthase Target

compound name	interaction	bond energy (kJ/mol)	bond length (Å)	compound name	interaction	bond energy (kJ/mol)	bond length (Å)
4(a)	Ser 205 (O)–N (11)	–1.61890	3.27622	4(k)	Arg 60 (N)–O (23)	–2.50000	2.99640
	Ser 205 (O)–N (12)	–2.50000	2.61902		Ser 205 (O)–O (26)	–2.39738	2.58769
	Arg 60 (N)–O (24)	–0.00775	2.29911		Arg 60 (N)–N (12)	–1.36329	2.79244
4(b)	Tyr 58 (N)–O (23)	–0.01189	3.57803	Arg 60 (N)–O (23)	–1.81084	2.55609	
	Asn 59 (N)–O (23)	–0.73913	2.59207	Tyr 204 (O)–O (23)	–0.26226	3.54755	
	Arg 60 (N)–O (23)	–2.50000	2.82512	Ser 205 (O)–O (23)	–2.49869	2.59998	
4(c)	Tyr 58 (N)–O (23)	–0.10649	3.44088	Arg 60 (N)–O (27)	–2.41387	3.09897	
	Asn 59 (N)–O (23)	–1.08913	2.58761	Arg 60 (N)–O (27)	–2.34329	3.12369	
	Arg 60 (N)–O (23)	–2.50000	3.09408	Arg 113 (N)–O (28)	–1.17171	2.90942	
	Ser 205 (O)–O (25)	–2.04184	2.54502	Arg 113 (N)–O (28)	–0.99612	3.11867	
4(d)	Tyr 58 (N)–O (23)	–0.09476	3.44893	4(l)	Arg 60 (N)–N (12)	–1.53196	3.08287
	Asn 59 (N)–O (23)	–1.06219	2.56740	Arg 60 (N)–O (24)	–0.85461	3.12642	
	Arg 60 (N)–O (23)	–2.49363	3.10127	Arg 60 (N)–O (24)	–1.99573	2.07049	
4(e)	Tyr 58 (N)–O (23)	–0.02610	3.54831	Tyr 204 (O)–O (24)	–1.22651	3.35470	
	Asn 59 (N)–O (23)	–0.65880	2.55617	Ser 205 (O)–O (24)	–0.11522	2.31383	
	Arg 60 (N)–O (23)	–2.50000	2.82583	Tyr 58 (N)–O (26)	–0.20459	3.10284	
4(f)	Ser 205 (O)–N (12)	–2.50000	3.00863	4(m)	Asn 59 (N)–O (26)	–2.48350	2.75736
	Arg 60 (N)–O (24)	–0.20808	3.15632	Tyr 58 (N)–O (23)	–0.01605	3.57054	
	Arg 60 (N)–O (24)	–1.35251	2.14446	Asn 59 (N)–O (23)	–0.92761	2.57293	
	Asn 59 (N)–N (25)	–0.25464	3.54907	Arg 60 (N)–O (23)	–2.50000	2.94743	
	Thr 63 (O)–N (25)	–2.41718	3.11656	4(n)	Tyr 58 (N)–O (23)	–0.08319	3.46818
	Thr 63 (O)–O (26)	–2.50000	2.60213	Asn 59 (N)–O (23)	–1.07656	2.57721	
	Asn 59 (N)–O (27)	–2.50000	2.60025	Arg 60 (N)–O (23)	–2.50000	3.08395	
4(g)	Asn 59 (N)–O (23)	–0.57469	2.64989	4(o)	Arg 60 (N)–N (12)	–2.48607	3.08471
	Arg 60 (N)–O (23)	–2.50000	2.61028	Arg 113 (N)–O (23)	–1.80969	2.61959	
	Asn 59 (N)–N (25)	–0.09783	3.58043	Tyr 58 (N)–N (26)	–1.66976	3.21718	
	Thr 63 (O)–N (25)	–1.10088	3.37982	Asn 59 (N)–O (27)	–2.05854	3.09542	
	Asn 59 (N)–O (26)	–2.50000	2.60122	Tyr 58 (N)–O (28)	–2.49951	2.71332	
	Thr 63 (O)–O (27)	–2.50000	2.80632	minodronic acid	Glu 93 (O)–O (11)	–2.50000	2.62058
	4(h)	Arg 60 (N)–N (12)	–1.49341	3.04388	Arg 60 (N)–O (15)	–2.20851	3.05595
Arg 60 (N)–O (24)	–0.84816	3.12660	Arg 60 (N)–O (15)	–2.22001	3.09973		
Arg 60 (N)–O (24)	–2.02485	2.06714	Glu 93 (O)–O (16)	–2.50000	2.64215		
	Tyr 204 (O)–O (24)	–1.20691	3.35862	Arg 113 (N)–O (16)	–0.35967	3.26586	
4(i)	Ser 205 (O)–O (24)	–0.17050	2.32046	Tyr 58 (N)–O (17)	–2.40243	2.62664	
	Ser 205 (O)–N (12)	–2.50000	2.88372	Glu 93 (O)–O (17)	–2.50000	2.70066	
	Arg 60 (N)–O (24)	–2.22715	3.10029	Arg 60 (N)–O (15)	–2.36085	3.09912	
4(j)	Glu 93 (O)–O (24)	–1.94256	3.21149	Asn 59 (N)–O (19)	–2.50000	2.60019	
	Tyr 58 (N)–O (23)	–0.05245	3.51506				
	Asn 59 (N)–O (23)	–0.99386	2.59110				

and limited commercial accessibility of phenylglyoxal derivatives, we prepared *in situ* phenylglyoxals from the phenyl methyl ketones in the presence of iodine on the basis of inference revealed from the literature.

To optimize the reaction conditions, a model condensation reaction of 2-aminopyridine **1(a)**, acetophenone **2(a)**, and dimedone (**3**) was performed in the presence and absence of varying catalysts and solvents under ultrasonic conditions. The initial reactions were carried out in the absence of an iodine source but did not result in our desired three-component product **4(a)** in both neat and water media even after 2 h (Table 1, entries 1 and 2). To explore the impact of varying iodine sources, the reaction was performed in the presence of sodium iodide, potassium iodide, copper iodide, and zinc iodide for 1 h, but the reaction did not proceed with substantial yields (Table 1, entries 3–6). It is noted from the data presented in Table 1 that the reaction of iodine in the water medium was found to be in a suitable condition to afford a trace amount of product in 79%

yield, while in the absence of water the medium had moderate performance to provide the product in a 62% yield even after one and half hours (Table 1, entries 7, 8).

After ascertaining the optimal reaction conditions, we found that in the presence of 20 mol % of iodine underwater medium the reaction proceeds efficiently to afford the product in a preminent yield (Table 1, entry 9). Intriguingly, the reaction was also executed for one and a half hours, but no further improvement in the yield of the product was acquired (Table 1, entry 10). A high amount of catalytic loading (25 mol %) under similar conditions revealed that there was no significant enhancement in the yield or in the reaction time (Table 1, entry 11). The results are summarized in Table 1.

In order to explore the generality and scope of this iodine-mediated multicomponent reaction, a wide variety of pertinent acetophenone, 2-amino pyridine derivatives, and dimedone was reacted under the optimized conditions, and the results are summarized in Table 2. Intriguingly, the 2-aminopyridine and

Table 5. Docking Scores^a of Imidazo[1,2-*a*]pyridin-3-yl Derivatives 4(a-o) Docked with Phosphodiesterase 3B Target Selected for Screening

compound name	MolDock score	rerank score (kJ/mol)	interaction energy (kJ/mol)	steric	HBond (kJ/mol)
4(a)	-108.136	-32.3135	-125.473	-118.475	-6.99816
4(b)	-111.562	-78.3614	-120.628	-116.517	-4.11087
4(c)	-119.362	-89.9521	-128.679	-124.015	-4.66410
4(d)	-116.080	-79.6175	-125.506	-120.981	-4.52482
4(e)	-111.031	-77.0171	-120.362	-116.213	-4.14992
4(f)	-118.320	-83.1092	-128.576	-119.230	-9.34526
4(g)	-130.663	-98.3234	-141.452	-132.962	-8.49026
4(h)	-109.303	-73.0475	-118.408	-114.611	-3.79774
4(i)	-115.557	-85.9591	-123.242	-119.762	-3.48020
4(j)	-118.900	-87.8734	-126.795	-120.784	-6.01043
4(k)	-128.312	-81.8875	-132.019	-122.726	-9.29270
4(l)	-116.616	-65.0245	-127.611	-118.031	-9.58031
4(m)	-115.537	-85.9622	-123.216	-119.743	-3.47298
4(n)	-126.841	-94.7604	-130.499	-122.702	-7.79698
4(o)	-125.361	-94.0195	-131.192	-126.334	-8.55344
olprinone	-105.404	-82.9526	-116.144	-112.107	-4.03755

^aMolDock score, rerank score, protein–ligand interaction, H-bond, and steric score.

Table 6. Molecular Interactions Analyses of Imidazo[1,2-*a*]pyridin-3-yl Derivatives 4(a-o) and Standard Drug with Phosphodiesterase 3B Target

compound name	interaction	bond energy (kJ/mol)	bond length (Å)	compound name	interaction	bond energy (kJ/mol)	bond length (Å)
4(a)	Ser 857 (O)–N (12)	-2.50000	3.04544	4(k)	Asn 860 (N)–O (23)	-1.01043	2.65725
	Asn 860 (O)–O (24)	-0.12746	3.57007		Leu 872 (O)–O (26)	-2.50000	2.75209
	Asn 860 (N)–O (24)	-1.87070	2.82732		Ser 857 (O)–N (12)	-2.50000	2.64745
4(b)	Ser 864 (O)–O (24)	-2.50000	2.79733	Asn 860 (N)–O (23)	-0.69619	2.81216	
	Ser 857 (O)–N (12)	-2.50000	2.79195	Ser 864 (O)–N (26)	-2.50000	2.71435	
	Asn 860 (N)–O (23)	-0.84588	2.79866	Asn 860 (N)–O (28)	-2.48162	3.10368	
4(c)	His 873 (N)–O (24)	-0.76499	3.44700	Ser 864 (O)–O (28)	-0.03093	2.31362	
	Ser 857 (O)–N (12)	-2.16410	3.16718	His 873 (N)–O (24)	-1.08396	3.38321	
	Leu 872 (O)–O (25)	-2.50000	2.73473	Ser 857 (O)–N (12)	-2.50000	2.89671	
4(d)	Ser 857 (O)–N (12)	-2.50000	2.80191	Asn 860 (N)–O (23)	-0.86219	2.61278	
	Asn 860 (N)–O (23)	-0.84081	2.71526	Ser 857 (O)–O (26)	-1.98567	3.20287	
	His 873 (N)–O (24)	-1.18401	3.36320	Ser 857 (O)–O (26)	-2.50000	2.61160	
4(e)	Ser 857 (O)–N (12)	-2.50000	2.80803	His 873 (N)–O (24)	-0.91767	3.41647	
	Asn 860 (N)–O (23)	-0.85524	2.76409	His 873 (N)–O (26)	-0.81479	3.43704	
	His 873 (N)–O (24)	-0.79468	3.44106	4(m)	Ser 857 (O)–N (12)	-2.50000	3.09672
4(f)	Ser 857 (O)–N (12)	-2.50000	3.04756	Asn 860 (N)–O (23)	-0.97299	2.64190	
	Ser 864 (O)–N (25)	-1.84526	3.23095	4(n)	Asn 860 (N)–N (11)	-0.02900	3.52202
	Ser 864 (O)–O (27)	-2.50000	2.60137	Ser 857 (O)–N (12)	-2.50000	3.01701	
4(g)	His 873 (N)–O (24)	-2.50000	2.92871	Asn 860 (N)–O (24)	-0.27708	2.92932	
	Ser 857 (O)–N (12)	-2.40937	3.11813	Tyr 844 (O)–O (26)	-2.49089	2.59891	
	Ser 864 (O)–N (25)	-2.42875	3.11425	His 853 (N)–O (26)	-2.50000	3.06206	
4(h)	Asn 860 (N)–O (26)	-1.15490	3.33927	4(o)	Asn 860 (N)–N (11)	-0.08751	3.51567
	Ser 864 (O)–O (27)	-2.49723	2.59967	Ser 857 (O)–N (12)	-1.47668	3.30466	
	Ser 857 (O)–N (12)	-2.50000	2.86090	Asn 860 (N)–O (24)	-0.14193	2.46943	
4(i)	Asn 860 (N)–O (23)	-0.87540	2.75165	Tyr 844 (O)–N (26)	-2.50000	2.60095	
	His 873 (N)–O (24)	-0.42234	3.51553	His 853 (N)–N (26)	-2.50000	3.02081	
	Ser 857 (O)–N (12)	-2.49607	3.10079	Tyr 844 (O)–O (27)	-1.84732	2.08756	
4(j)	Asn 860 (N)–O (23)	-0.98413	2.66454	olprinone	Ser 857 (O)–N (8)	-1.53755	3.29249
	Ser 857 (O)–N (12)	-2.50000	3.07232	Ser 864 (O)–O (15)	-2.50000	3.08748	

derivative tethered with methyl at the para position were reacted under the optimized reactions, and in all of the cases significant yields were obtained. The variability of acetophenone derivatives having substituents such as 4-Cl, 2-OH, 4-OH, 4-OMe, 4-Br, 4-NO₂, and 3-NO₂ was found suitable for the synthesis of the corresponding imidazole-fused pyridine-3yl

tethered with dimedone scaffolds. It should be noted that the acetophenone substituted with electron-donating groups resulted in better yields as compared to electron-withdrawing groups. It is noteworthy to mention that under the given reaction conditions; we did not observe any iodination in the

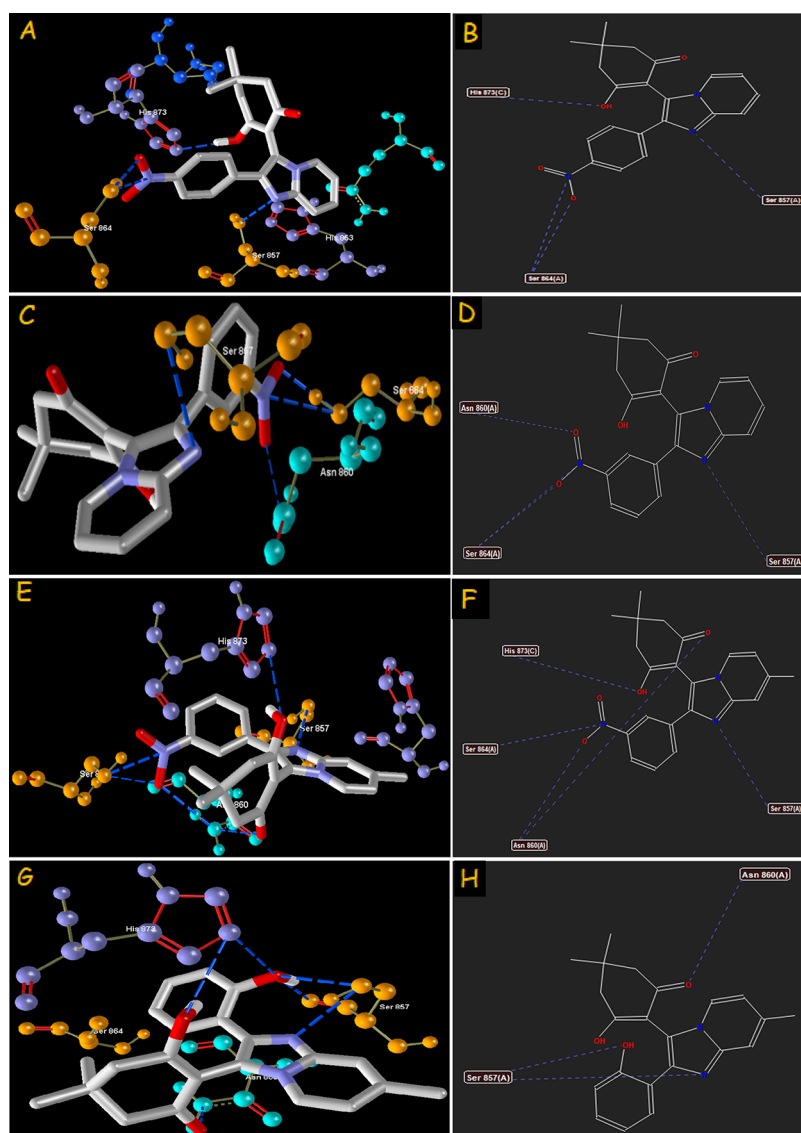


Figure 5. Hydrogen-bond interaction of compounds 4(f) (A–B), 4(g) (C–D), 4(k) (E–F), and 4(l) (G–H) with the phosphodiesterase 3B target.

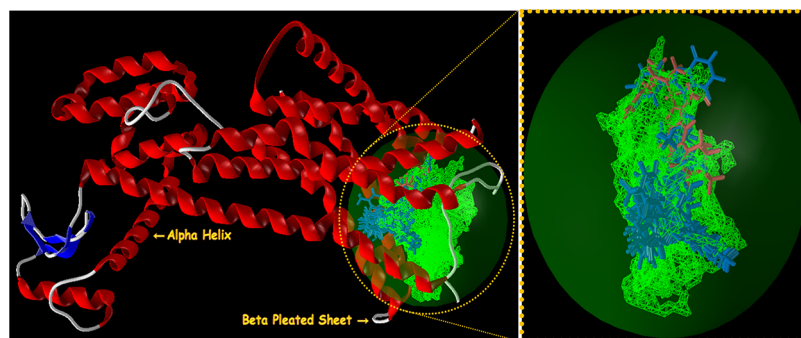


Figure 6. Secondary structure of CXCR4 binds with imidazo[1,2-a]pyridin-3-yl derivatives 4(a–o) (blue) and standard drug GSK812397 (pink) inside the cavity (green framework).

aromatic rings of products 4(a–o). Also, the benzylic CH_2 of the indene was unaffected by the iodine-mediated oxidation process.

To check the feasibility of scale-up and efficiency of this protocol, gram-scale synthesis of 3-hydroxy-2-(2-(4-methoxyphenyl)imidazo[1,2-a]pyridin-3-yl)-5,5-dimethylcyclohex-2-enone 4(d) was carried out under optimized reaction

conditions. The condensation reaction of imidazole-fused pyridin-3-yl substrate in the 5 mmol scale resulted in the corresponding yield of 1.757 g with 91% yield.

On the basis of inference revealed from the literature and resultant outcomes,^{41,42} a plausible mechanistic pathway for the molecular iodine-catalyzed synthesis of imidazo[1,2-a]pyridin-

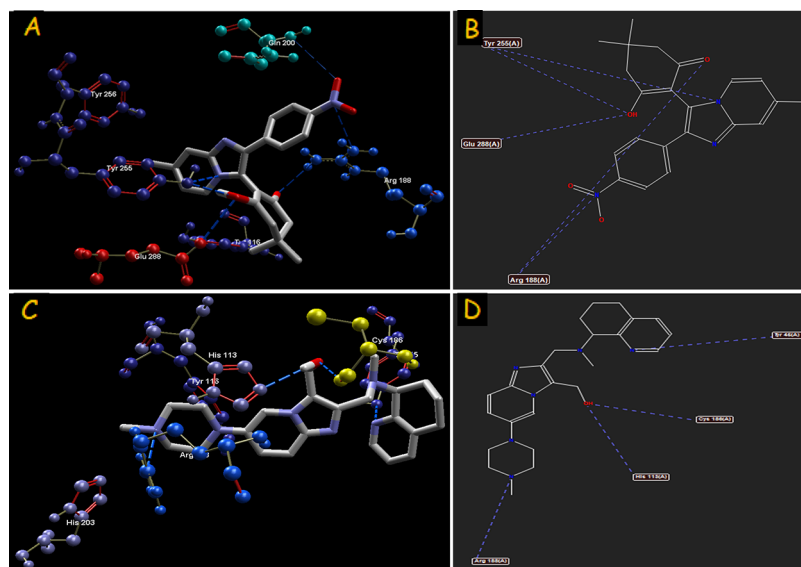


Figure 7. Hydrogen-bond interaction of compounds 4(o) (A–B) and standard drug GSK812397 (C–D) with the CXCR4 target.

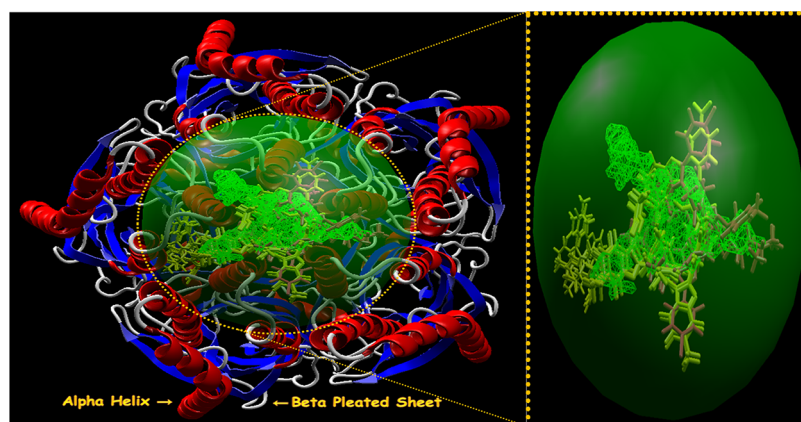


Figure 8. Secondary structure of GABAa agonist binds with imidazo[1,2-a]pyridin-3-yl derivatives 4(a-o) (yellow) and standard drugs (pink) inside the cavity (green framework).

3-yl derivatives 4(a-o) is depicted in Scheme 2. The cascade reaction began with the attack of molecular iodine on acetophenone derivatives 2(a-g) in an aqueous medium followed by dehydration which resulted *in situ* generation of phenylglyoxal (1'). The Knoevenagel-type reaction takes place between phenylglyoxal (1') and enolic form (3') of dimedone (3) to form an intermediate (5') followed by the elimination of water molecule. Furthermore, the 2-aminopyridine 1(a-b) undergoes aza-Michael addition to form adduct (6), which subsequently undergoes intramolecular ring closure via an energetically favored 5-*exo-trig* process, thereby resulting in the cycloadduct (7) followed by removal of water that furnishes the desired product 4(a-o). The whole process involves the elimination of three molecules of water as a greener waste.

Iodine can act as either a Lewis acid or as a source of *in situ* HI in organic transformations. To be acquainted with the concrete function of iodine via a three-component reaction, a few additional experiments were conducted. The model condensation reaction of 2-aminopyridine 1(a), acetophenone 2(a), and dimedone (3) was performed using 20 mol % HI in water media to afford the product 4(a) in a moderate yield of 67%. To abandon the role of *in situ* HI, we executed a further reaction in the presence of iodine (20 mol %) along with 20 mol % of

sodium hydrogen carbonate under aqueous media in similar reaction conditions. Interestingly, this resulted in 88% of the tetrasubstituted imidazo[1,2-a]pyridin-3-yl linked with a dimedone ring 4(a). It is noteworthy to mention that, if the reaction is catalyzed by HI in the presence of an equimolar amount of base, it will nullify the acid and have a drastic effect on the yield of the desired product. Since in our protocol this did not happen, we believe that iodine is acting as a Lewis acid to activate the carbonyl group (CO) in all the steps involves in a plausible mechanism as shown in Scheme 2.

3.2. Molecular Docking Studies. The secondary structures of farnesyl diphosphate synthase and the phosphodiesterase 3B target with the detected active sites are presented in Figures 2 and 4, respectively. The screening results against the farnesyl diphosphate synthase target showed that compound 4(k) exhibited the highest MolDock score (−145.600), rerank score (−107.580), and protein–ligand interaction (−149.188) among the series, and a comparable steric score (−136.328) with compound 4(g) demonstrating the highest steric score (−139.207) among the series. In comparison with the reference standard minodronic acid, all compounds in the series demonstrated a better MolDock score, protein–ligand energy,

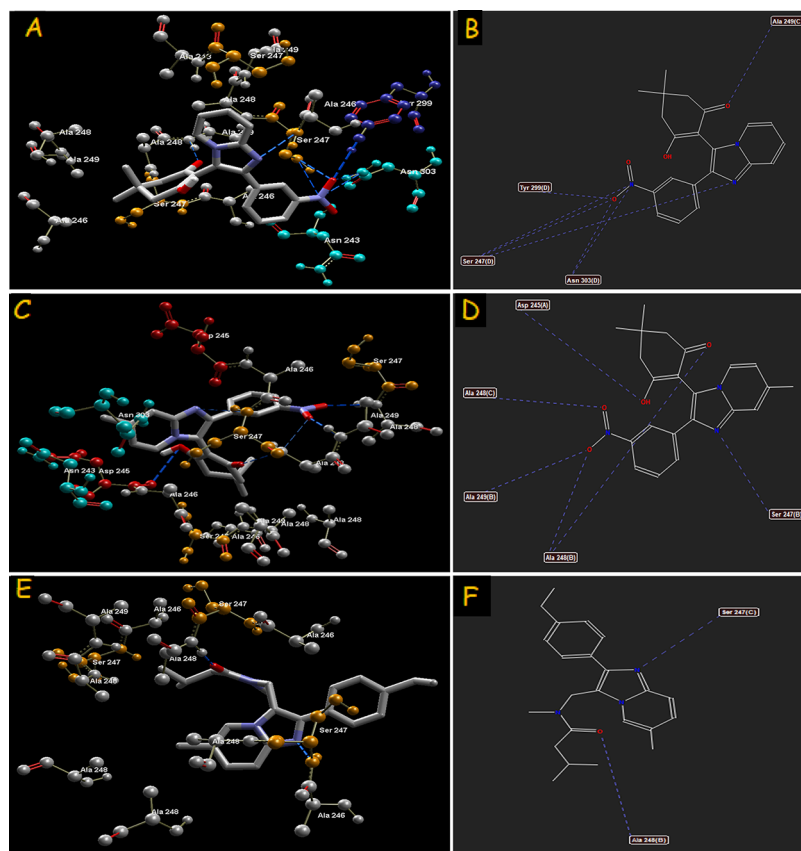


Figure 9. Hydrogen-bond interaction of compounds 4(g) (A–B), 4(k) (C–D), and standard drug necopidem (E–F) with the GABA_A target.

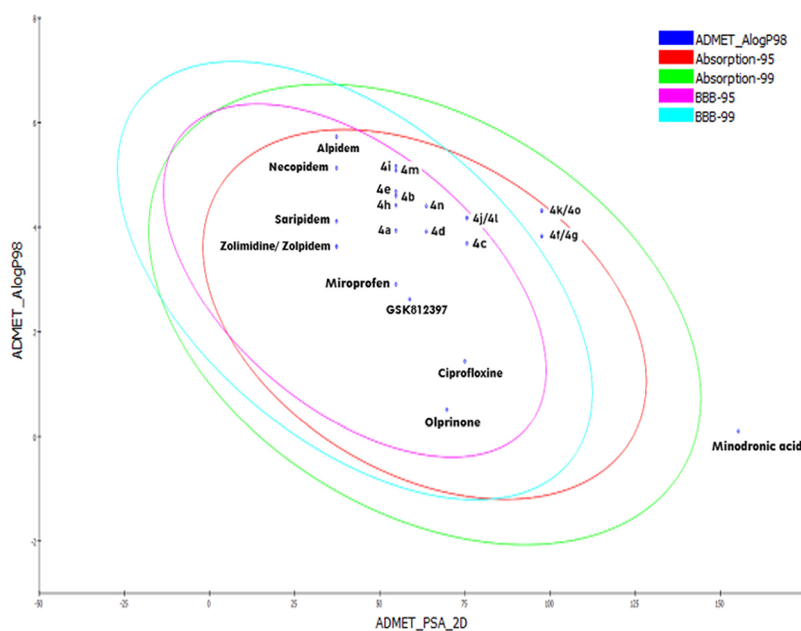


Figure 10. A plot of AlogP98 versus 2D polar surface area (PSA) for the synthesized compounds 4(a–o) and standard drugs.

and steric scores against farnesyl diphosphate synthase as summarized in Table 3.

The compounds 4(k), 4(g), and 4(l) with the highest moldock, rerank scores, steric scores, and protein–ligand energy reveal that the substitutions on the aromatic ring by nitro and hydroxyl groups at the meta and ortho positions respectively show significant binding affinity with the farnesyl diphosphate

synthase target. The hydrogen-bond interactions, bond length, and bond energies of imidazo[1,2-*a*]pyridin-3-yl derivatives and standard drug minodronic acid are depicted in Table 4. All of the compounds and minodronic acid shows H-bond interactions with Tyr 58, Asn 59, Arg 60, Thr 63, Glu 93, Arg 113, Tyr 204, and Ser 205 of the farnesyl diphosphate synthase target. The

Table 7. Absorption, Distribution, Metabolism, Excretion, and Toxicity (ADMET) Predictions for the Synthesized Compounds 4(a-o) and Standard Drugs

compounds	BBB level ^a	absorption level ^b	hepatotoxicity ^c	CYP2D6 ^d	PPB ^e	solubility ^f	AlogP98 ^g	PSA 2D
4a	1	0	0	0	true	-5.186	3.932	54.725
4b	1	0	0	1	true	-5.896	4.596	54.725
4c	2	0	0	0	false	-4.686	3.690	75.541
4d	1	0	0	0	true	-5.199	3.915	63.655
4e	1	0	0	0	true	-5.972	4.680	54.725
4f	4	0	0	0	true	-5.326	3.826	97.548
4g	4	0	0	0	true	-5.350	3.826	97.548
4h	1	0	0	1	true	-5.668	4.418	54.725
4i	1	0	0	0	true	-6.449	5.166	54.725
4j	2	0	0	0	true	-5.162	4.176	75.541
4k	4	0	0	0	true	-5.818	4.312	97.548
4l	2	0	0	0	true	-5.141	4.176	75.541
4m	1	0	0	1	true	-6.374	5.082	54.725
4n	1	0	0	0	true	-5.671	4.402	63.655
4o	4	0	0	0	true	-5.793	4.312	97.548
Alpidem	0	0	0	0	true	-6.455	5.729	37.262
Ciprofloxacin	3	0	0	0	false	-3.162	1.435	74.932
GSK812397	2	0	0	0	true	-3.910	2.621	58.743
minodronic acid	4	3	0	0	false	-1.462	0.098	155.288
miroprofen	2	0	0	0	true	-3.750	2.905	54.725
necopidem	0	0	0	0	true	-6.072	5.130	37.262
olprinone	3	0	0	0	false	-2.255	0.509	69.655
saripidem	1	0	0	0	true	-5.174	4.114	37.262
zolimidine	2	0	0	0	true	-3.812	2.304	51.210
zolpidem	1	0	0	0	true	-4.984	3.628	37.262

^a0, 1, 2, 3, and 4 denote very high, high, medium, low, and undefined, respectively. ^b0, 1, 2, and 3 denote good absorption, moderate absorption, low absorption, and very low absorption, respectively. ^c0 and 1 represent nontoxic and toxic, respectively. ^d0 and 1 denote noninhibitor and inhibitor, respectively. ^eTrue symbolizes binding, and false symbolizes nonbinding of the drug. ^f-6.0 to -4.0, -4.0 to -2.0, and -2.0 to 0.0 represents low, good, and optimal solubility, respectively. ^gAlogP98 > 5 indicates good absorption through BBB.

Table 8. Toxicity Prediction of All the Synthesized Compounds 4(a-o)

compounds	rat male NTP ^a prediction	mouse male NTP ^a prediction	Ames mutagenicity prediction	skin irritation	aerobic biodegradability prediction
4a	non-carcinogen (0.000)	non-carcinogen (0.000)	non-mutagen (0.000)	non-irritant (0.000)	non-biodegradable (0.000)
4b	non-carcinogen (0.000)	non-carcinogen (0.000)	non-mutagen (0.000)	non-irritant (0.000)	non-biodegradable (0.000)
4c	non-carcinogen (0.010)	non-carcinogen (0.000)	non-mutagen (0.000)	non-irritant (0.000)	non-biodegradable (0.000)
4d	non-carcinogen (0.000)	non-carcinogen (0.000)	non-mutagen (0.000)	non-irritant (0.000)	non-biodegradable (0.000)
4e	non-carcinogen (0.001)	non-carcinogen (0.000)	non-mutagen (0.094)	non-irritant (0.000)	non-biodegradable (0.000)
4f	non-carcinogen (0.001)	non-carcinogen (0.000)	non-mutagen (0.022)	non-irritant (0.000)	non-biodegradable (0.000)
4g	non-carcinogen (0.000)	non-carcinogen (0.000)	non-mutagen (0.000)	non-irritant (0.003)	non-biodegradable (0.131)
4h	non-carcinogen (0.000)	non-carcinogen (0.000)	non-mutagen (0.000)	non-irritant (0.000)	biodegradable (1.000)
4i	non-carcinogen (0.000)	non-carcinogen (0.000)	non-mutagen (0.000)	non-irritant (0.002)	non-biodegradable (0.000)
4j	non-carcinogen (0.001)	non-carcinogen (0.000)	non-mutagen (0.002)	non-irritant (0.000)	non-biodegradable (0.000)
4k	non-carcinogen (0.000)	non-carcinogen (0.000)	non-mutagen (0.000)	non-irritant (0.030)	non-biodegradable (0.000)
4l	non-carcinogen (0.000)	non-carcinogen (0.000)	non-mutagen (0.000)	non-irritant (0.000)	non-biodegradable (0.000)
4m	non-carcinogen (0.009)	non-carcinogen (0.000)	non-mutagen (0.000)	irritant (0.992)	non-biodegradable (0.000)
4n	non-carcinogen (0.001)	non-carcinogen (0.000)	non-mutagen (0.008)	non-irritant (0.000)	non-biodegradable (0.002)
4o	non-carcinogen (0.000)	non-carcinogen (0.000)	non-mutagen (0.000)	non-irritant (0.000)	non-biodegradable (0.016)

^aNTP: National Toxicology Program.

reference drug exhibits the highest H-bond interactions followed by compound 4(k) (-19.5515 and -12.8601, respectively).

It is inferred from Table 5 that, among the imidazo[1,2-*a*]pyridin-3-yl derivatives, compound 4(g) showed the highest MolDock (-130.663), rerank (-98.323), protein-ligand energy (-141.452), and steric (-132.962) scores against phosphodiesterase 3B. All of the compounds in the series exhibited a greater MolDock score, protein-ligand energy, and steric score when compared with the reference standard

olprinone. The rerank scores of the remaining compounds in the series except for 4(a), 4(b), 4(d), 4(e), 4(h), 4(k), and 4(l) are also better than that of olprinone. It should be noted from Table 5 that the presence of substitutions on the aromatic ring at the meta position followed by the para position enhances the binding affinities of the ligand and the protein. The hydrogen-bond interactions of all the compounds 4(a-o) and reference standard olprinone, with Tyr 844, Ser 857, Asn 860, Ser 864, Leu 872, and His 873, of the phosphodiesterase 3B target are

Table 9. Physicochemical Properties of All of the Synthesized Compounds 4(a-o) and Standard Drugs on the Basis of Lipinski's Rule of Five^a

compounds	MW (g/mol)	nHBA	nHBD	TPSA (Å ²)	Log P _{o/w}	nLV
4a	332.40	3	1	54.60	3.56	0
4b	366.84	3	1	54.60	4.12	0
4c	348.40	4	2	74.83	3.18	0
4d	362.42	4	1	63.83	3.59	0
4e	411.29	3	1	54.60	4.19	0
4f	377.39	5	1	100.42	2.85	0
4g	377.39	5	1	100.42	2.84	0
4h	346.42	3	1	54.60	3.89	0
4i	425.32	3	1	54.60	4.54	0
4j	362.42	4	2	74.83	3.49	0
4k	391.42	5	1	100.42	3.20	0
4l	362.42	4	2	74.83	3.45	0
4m	380.87	3	1	54.60	4.45	0
4n	376.45	4	1	63.83	3.91	0
4o	391.42	5	1	100.42	3.21	0
alpidem	404.33	2	0	37.61	4.89	0
ciprofloxacin	331.34	5	2	74.57	1.10	0
GSK812397	402.35	7	1	60.14	2.44	0
minodronic acid	680.79	8	5	172.21	-1.74	0
miroprofen	266.29	3	1	54.60	2.64	0
necopidem	363.50	2	0	37.61	4.40	0
olprinone	250.26	3	1	73.95	1.67	0
saripidem	341.83	2	0	37.61	3.66	0
zolimidine	272.32	3	0	59.82	2.25	0
zolpidem	307.39	2	0	37.61	3.13	0

^aMW molecular weight, nHBD number of hydrogen-bond donor, nHBA number of hydrogen-bond acceptor, TPSA topological polar surface area, Log P_{o/w} octanol/water partition coefficient, nLV number of Lipinski violation.

summarized in Table 6. The compounds 4(l) (-9.58031) followed by 4(f) (-9.34526), 4(k) (-9.29270), and 4(g) (-8.49026) exhibit the highest H-bond interaction among the series and reference drug.

The screening of the imidazo[1,2-*a*]pyridin-3-yl derivatives against the target CXCR4 revealed that all the compounds exhibited inferior docking scores (MolDock score, rerank score, protein–ligand energy, and steric score) when compared with the reference standard GSK812397. The H-bond interactions with bond length and energies are depicted in Table 2S of Supporting Information. The compound 4(o) followed by GSK812397 demonstrates high H-bond interactions (-9.5484 and -8.9460, respectively) among the series. Tyr 45, His 113, Thr 117, Cys 186, Arg 188, Gln 200, His 203, Tyr 255, Tyr 256, and Glu 288 of the CXCR4 target exhibit H-bond interactions with all of the compounds and GSK812397 target. The secondary structures for CXCR4 and GABA_A are depicted in Figures 6 and 8, respectively.

For GABA_A agonistic activity, compound 4(k) showed the highest MolDock score and protein–ligand energy (-127.861 and -132.945, respectively) followed by 4(g) (-127.803 and -132.640, respectively), while reference standard Necopidem exhibited the highest rerank and steric scores (-87.3621 and -126.952, respectively) followed by compound 4(g) (-78.484 and -125.020, respectively). The hydrogen-bond interactions, bond length, and bond energy of compounds and standard drugs alpidem, necopidem, saripidem, and zolpidem are summarized in Table 4S of Supporting Information. The compounds 4(g) followed by 4(k) exhibit the highest H-bond interactions (-11.6198 and -9.79576, respectively) among the series and as compared to reference drugs. All of the compounds and reference drugs show H-bond interactions with the Asp 48, Val 50, Ser 51, Glu 52, Gln 185, Arg 216, Asp 245, Ser 247, Ala 248, Ala 249, Lys 274, Tyr 299, and Asn 303 of the GABA_A agonist target.

However, the data need further experimental support to establish the selectivity profile of the imidazo[1,2-*a*]pyridin-3-yl derivatives. The binding interactions (H-bond and steric) of compound 4(k) with farnesyl diphosphate synthase and 4(g) with phosphodiesterase 3B are portrayed in Figures 3 and 5, respectively. The H-bond interactions of CXCR4 and GABA_A with amino acids are illustrated in Figures 7 and 9, respectively. It can be postulated from the overall screening data (Tables 3 and 5) that compounds 4(k) and 4(g) exhibited the highest selectivity with farnesyl diphosphate synthase and phospho-

Table 10. Electron Density-Based Molecular Properties Calculated with the DFT/B3LYP/6-311G++(d,p) Level of Theory for Imidazo[1,2-*a*]pyridin-3-yl Derivatives 4(a-o)^a

compounds	E_{HOMO} (eV)	E_{LUMO} (eV)	$\Delta E = E_{(\text{LUMO}-\text{HOMO})}$ (eV)	η (eV)	μ (eV)	ω (eV)
4(a)	-5.3878	-1.4150	3.9728	1.9864	-3.4014	2.9122
4(b)	-5.5511	-1.5238	4.0273	2.0137	-3.5375	3.1072
4(c)	-5.2790	-1.3878	3.8912	1.9456	-3.3334	2.8556
4(d)	-5.4151	-1.6055	3.8096	1.9048	-3.5103	3.2345
4(e)	-5.5239	-1.5238	4.0001	2.0001	-3.5239	3.1043
4(f)	-5.8232	-2.4218	3.4014	1.7007	-4.1225	4.9965
4(g)	-5.7144	-2.2858	3.4286	1.7143	-4.0001	4.6669
4(h)	-5.2790	-1.3606	3.9184	1.9592	-3.3198	2.8126
4(i)	-5.4151	-1.4966	3.9185	1.9593	-3.4559	3.0478
4(j)	-5.1702	-1.3606	3.8096	1.9048	-3.2654	2.7989
4(k)	-5.6055	-2.2585	3.3470	1.6735	-3.9320	4.6192
4(l)	-5.1702	-1.2517	3.9185	1.9593	-3.2110	2.6312
4(m)	-5.4151	-1.4966	3.9185	1.9593	-3.4559	3.0478
4(n)	-5.1429	-1.3334	3.8095	1.9048	-3.2382	2.7525
4(o)	-5.6872	-2.3674	3.3198	1.6599	-4.0273	4.8856

^a(η) Chemical hardness, (ω) electrophilicity index of molecules, and (μ) electronic chemical potential.

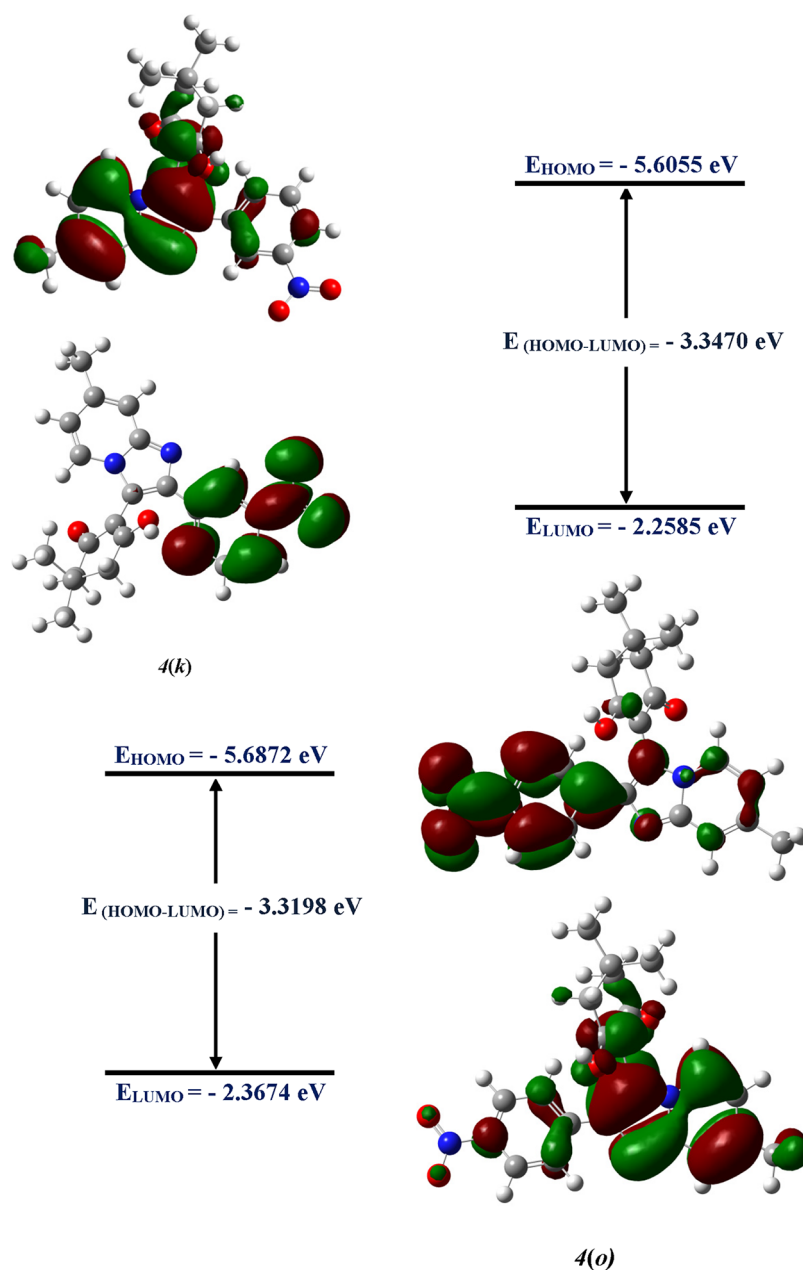


Figure 11. Optimized geometries with a frontier molecular orbital of 4(k) and 4(o).

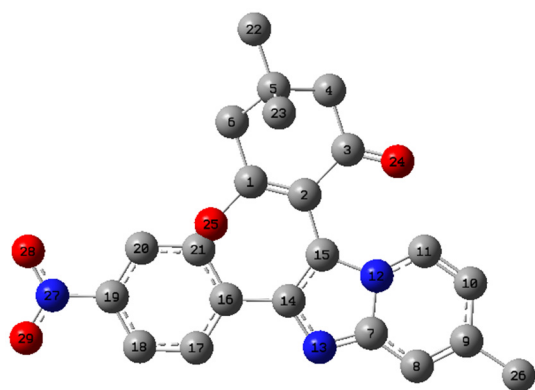


Figure 12. Labeled image of atoms for compound 4(o).

diesterase 3B, respectively, among the series in terms of the MolDock score, and the other imidazo[1,2-*a*]pyridin-3-yl derivatives demonstrated comparable binding affinity against farnesyl diphosphate synthase and phosphodiesterase 3B in terms of overall docking scores (MolDock score, rerank score, protein–ligand energy, and steric score).

3.3. Prediction of ADMET, Toxicity, and Drug-Likeness Properties. The pharmacokinetic profiles of all of the synthesized compounds 4(a-o) and standard drugs under investigation were envisioned by ADMET (absorption, distribution, metabolism, excretion, and toxicity) models provided by the Discovery Studio 2019 program.³² The biplot exhibits the two analogous 95% and 99% confidence ellipses corresponding to the human intestinal absorption (HIA) and the blood–brain barrier (BBB) models, respectively, as depicted in Figure 10. The plot presents green and blue ellipses with 99% confidence limits, whereas the red and pink ellipses show 95%

Table 11. Local Reactivity Descriptors for Compound 4(o) in Terms of Fukui Function Using DFT/B3LYP/6-311G++ (d, p) Level of Theory

atom	$q_k(N)$	$q_k(N+1)$	f_k^+	f_k^-	f_k^0
C ₁	-0.151310	-0.38542	-0.401360	0.250047	0.007970
C ₂	-0.092970	0.42033	0.249521	-0.342490	0.085405
C ₃	0.238183	-0.47370	-0.483440	0.721625	0.004871
C ₄	0.184695	-0.22889	-0.304330	0.489020	0.037720
C ₅	-0.362620	0.29922	0.587872	-0.950490	-0.144325
C ₆	0.174867	-0.12933	-0.309850	0.484712	0.090258
C ₇	0.312993	0.10023	0.122315	0.190678	-0.011042
C ₈	0.018006	0.23488	0.088316	-0.070310	0.073283
C ₉	-0.081770	0.11073	0.221697	-0.303470	-0.055486
C ₁₀	-0.054300	0.09544	-0.083020	0.028717	0.089229
C ₁₁	0.218577	-0.13781	-0.092950	0.311523	-0.022431
N ₁₂	-0.355590	0.29693	0.247717	-0.603310	0.024607
N ₁₃	-0.378090	0.08790	0.007784	-0.385870	0.040059
C ₁₄	0.061015	-0.355810	-0.393740	0.454753	0.018966
C ₁₅	0.104763	0.091094	0.097453	0.007310	-0.003180
C ₁₆	-0.163560	0.659550	0.587435	-0.750990	0.036058
C ₁₇	0.119294	-0.270240	-0.435790	0.555082	0.082774
C ₁₈	0.033791	0.474118	0.331978	-0.298190	0.071070
C ₁₉	0.210717	-0.463470	-0.462950	0.673667	-0.000261
C ₂₀	-0.217070	-0.798400	-0.934870	0.717799	0.068236
C ₂₁	0.364037	-0.545010	-0.431450	0.795488	-0.056778
C ₂₂	0.128279	0.214642	0.058900	0.069379	0.077871
C ₂₃	0.138569	0.009307	-0.145230	0.283802	0.077270
O ₂₄	-0.344970	-0.018290	-0.188560	-0.156420	0.085135
O ₂₅	0.201408	1.660380	1.485765	-1.284360	0.087308
C ₂₆	0.114567	0.167997	0.018904	0.095663	0.074547
N ₂₇	0.123946	-0.227000	-0.256400	0.380350	0.014704
O ₂₈	-0.229870	0.098736	-0.026610	-0.203250	0.062675
O ₂₉	-0.315590	0.011858	-0.155120	-0.160470	0.083489

confidence limits for the intestinal absorption (HIA) and blood–brain barrier (BBB), respectively.^{33,43,44} The screened results of ADMET comprised of some descriptors such as the blood–brain barrier (BBB), absorption, solubility, hepatotoxicity, cytochrome P₄₅₀ 2D6 (CYP2D6), plasma protein binding (PPB), AlogP98, and PSA2D are summarized in Table 7.

According to the ADMET prediction, four of the compounds 4(f–g), 4(k), and 4(o) were outside the 99% BBB confidence ellipse, meaning that the quality of the results obtained were unknowable (undefined level of 4). All of the compounds 4(a–o) and standard drugs except minodronic acid were inside the 99% absorption ellipse that revealed the good intestinal absorption of the compounds. The obtained AlogP98 values of all the compounds, except 4(i) and 4(m), were found to be less than five, which divulges the easy absorption of the drug through the blood–brain barrier.⁴⁴ The two standard drugs alpidem, and necopidem indicate the higher value of atom-based Log P98 among the standard drugs and all of the synthesized compounds 4(a–o).

The cytochrome P450 2D6 (CYP2D6) is intricate in the metabolism of a varied range of xenobiotics, and its inhibition by a drug may lead to serious drug–drug interactions. Consequently, determining the CYP2D6 inhibition is a vital part of the drug discovery and development process.⁴³ All of the compounds, except 4(b), 4(h), and 4(m), were classified as noninhibitors of CYP2D6. The hepatotoxicity model predicts the occurrence of dose-dependent human toxicity. According to the hepatotoxicity model, all of the compounds and standard drugs were classified as non-hepatotoxic. All of the synthesized

compounds show low solubility, as compared to the standard drugs assorted from lower to optimal solubility. The pharmaceutical activity is determined by the free drug concentration; therefore, the possible plasma protein binding of compounds must be considered.⁴³ All of the synthesized compounds were likely to be binding, whereas only 4(c) was likely to be nonbinding among the synthesized library of compounds.

The toxicity predictions of the synthesized compounds 4(a–o) were also investigated with Discovery Studio 2019 using the toxicity prediction by a komputer-assisted technology (TOPKAT) protocol.^{32,33} The acquired outcomes of the TOPKAT protocol are summarized in Table 8. The predicted toxicity values are in the range of 0.0–0.30, 0.30–0.70, and 0.70–1.0 representing the nontoxic, interval, and toxic nature of the drugs, respectively.³³ The resultant toxicity parameters revealed the potency of all the synthesized compounds, except 4(h) and 4(m) with less toxicity and a greater safety index. The toxicity predictions of all of the compounds were endowed to be preferable for the development of this synthesized library of compounds into medicinal drugs.

To determine the ability of the drug to diffuse passively through the BBB, analyses of drug-likeness were performed by Lipinski's rule-of-five prediction of the drug. The rule states that a compound can be considered biologically active for an oral administration in humans if it does not violate more than one of these thresholds: the molecular weight (MW) of the molecule must be <500 Da, octanol/water partition coefficient (iLOGP) must be ≤5, number of hydrogen-bond acceptors (nHBA) must

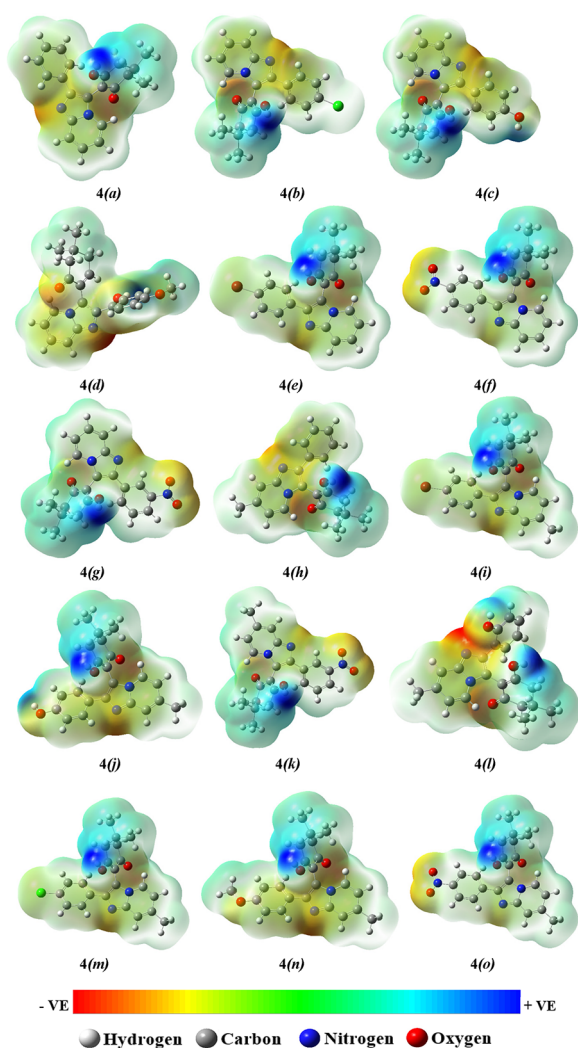


Figure 13. Molecular electrostatic potential (MEP) maps of the synthesized compounds 4(a–o).

be ≤ 10 , number of hydrogen-bond donors (nHBD) ≤ 5 , and topological polar surface area (TPSA) $\leq 40 \text{ \AA}^2$.⁴⁵ To ascertain the drug-likeness character of compounds, the Discovery Studio 2019 program was used for determining the substantial pharmacokinetic properties.^{32,33} The outputs of drug-likeness properties of synthesized compounds 4(a–o) in comparison with standard drugs are summarized in Table 9. The results reveal that the synthesized imidazo[1,2-*a*]pyridine derivatives 4(a–o) have zero violations of Lipinski's rule.

3.4. Frontier Molecular Orbital Analysis. The frontier orbital of the chemical compounds is a very significant parameter in drug design and in recognizing their reactivity.^{46–48} The higher value of the highest occupied molecular orbital (HOMO) of a molecule can donate electrons to suitable acceptor molecules with low energy and empty molecular orbitals (LUMO). The predicted frontier orbital energies, the chemical potential (μ),³⁶ chemical hardness (η),⁴⁹ and electrophilicity index (ω)^{37,50} are summarized in Table 10.

All the molecular structures of imidazo[1,2-*a*]pyridin-3-yl derivatives 4(a–o) were optimized utilizing the level of theory as mentioned in the Experimental Section.³⁴ After optimization of all the structures, the vibrational modes were checked to be true energy minima by frequency analyses, and it revealed that no imaginary frequencies were observed. The chemical hardness

(η) shows the reactivity of the molecule, where a larger η value indicates a less reactive nature than a molecule having a smaller value of η . A hard molecule that possesses a large HOMO–LUMO gap means high excitation energies are required to manifold excited states and be less reactive, and their electron density is less easily changed than a soft molecule.⁵¹

The FMOs distribution patterns at the ground state of imidazo amalgamated pyridine hybrid molecules 4(k) and 4(o) are depicted in Figure 11. All the optimized geometries with a frontier molecular orbital of 4(a–j) and 4(l–n) are portrayed in Figure 2S of the Supporting Information. The trend of the hardness of molecules in the following increasing order:

$$4(\mathbf{o}) < 4(\mathbf{k}) < 4(\mathbf{f}) < 4(\mathbf{g}) < 4(\mathbf{d}) = 4(\mathbf{j}) = 4(\mathbf{n}) < 4(\mathbf{c}) \\ < 4(\mathbf{h}) < 4(\mathbf{i}) = 4(\mathbf{l}) = 4(\mathbf{m}) < 4(\mathbf{a}) < 4(\mathbf{b}) < 4(\mathbf{e})$$

The trend of chemical hardness reveals that compound 4(e) is the least reactive, while the compounds 4(o), 4(k), 4(f), and 4(g), respectively, are the most reactive molecules among the series of imidazo-pyridine derivatives. The electrophilicity index (ω) divulges the stabilization energy when the system is augmented by an electronic charge from the surrounding environment.⁵⁰ Furthermore, the calculated results also indicate that the imidazo-pyridine hybrid molecules substituted with a nitro functional group on the aryl are more reactive and hence are more active as highlighted in the *in silico* studies for compounds 4(o), 4(k), 4(f), and 4(g) with the nitro group substitution found to be more potent against the farnesyl diphosphate synthase, human phosphodiesterase 3B, CXCR4, and GABAa agonist targets. Thus, the result obtained from the DFT studies by the level of theory used is qualitatively only and in good agreement with the outcomes of *in silico* analyses.

3.5. Local Reactivity Descriptors and Electrostatic Potential Surface Analysis. To predict the reactivity and selectivity, the local reactivity descriptors such as Fukui functions (f_k^+ , f_k^- , and f_k^0) were calculated at the DFT/B3LYP/6-311G++ (d, p) level of theory for the synthesized compound 4(o) using the natural bond order (NBO) analysis method.³⁹ The labeled image of the atoms for 4(o) is depicted in Figure 12.

The charges extant on each atom were calculated as qk (k th atom) for the cationic ($N - 1$), anionic ($N + 1$), and neutral (N) molecule of the compound 4(o). The atomic sites likely to undergo electrophilic and nucleophilic attacks can be ascertained using the highest value of the Fukui function for the HOMO (f_k^-) and LUMO (f_k^+), respectively.⁴⁰ The local reactivity descriptors for compound 4(o) in terms of Fukui functions are summarized in Table 11. The highest value of the Fukui function for the LUMO (f_k^+) is 1.4858 followed by 0.5879 present around the atoms O₂₅ and C₅, which indicates the most electrophilic sites, respectively, and these are the probable sites for nucleophilic attacks. However, the atom C₂₁ characterized by the highest value of the Fukui function for the HOMO (f_k^-) is 0.7955, which represents the nucleophilic site and hence possible site for the electrophilic attack. The highest value of the Fukui function for the (f_k^0) is 0.0903 present around atom C₅, which reveals the most significant site for the radical attacks.

The molecular electrostatic potential surface to envisage the reactive sites in the optimized structure of all of the synthesized compounds 4(a–o) is mapped in Figure 13. The red color in the map signifies an electronegative region with minimum electrostatic potential that divulges its susceptibility to electrophilic

attack. Similarly, the blue color represents an electropositive region liable for the nucleophilic attack, whereas green is a region of zero potential.^{52,53} The MEP diagrams revealed that the red region corresponds to the oxygen atom of the carbonyl group of dimedone, imine group of the imidazole ring, and oxygen atoms of substituted nitro, hydroxyl, and methoxy groups of the acetophenone ring, which indicates its most reactivity toward the intermolecular hydrogen-bonding interactions. The hydrogen atoms of the hydroxyl group of the dimedone ring exhibit the electropositive nature as represented in blue regions.

4. CONCLUSION

An ultrasonic-assisted efficient and environmentally sustainable methodology is presented for the synthesis of pharmacologically significant 2-phenylimidazo[1,2-*a*]pyridine-3-yl scaffolds. The molecular-iodine-catalyzed protocol for the synthesis of biologically active synthetic equivalents has been envisaged to intensify the viability and yield of the products. The higher environmental compatibility and sustainability factors of this protocol thereby satisfy the triple bottom line philosophy of green and sustainable chemistry. The reaction protocol is also feasible for the multigram scale, which devises an economically affordable methodology on a large scale.

The virtual screening of synthetic moieties against several biological targets attributed significant interactions with the active site of receptor proteins. The compounds **4(k)** and **4(g)** have come to light as potential inhibitors with the highest selectivity against farnesyl diphosphate synthase and phosphodiesterase 3B, respectively. The acquired results indicate that the theoretical studies are in good agreement with the outcomes of *in silico* analyses. This screening study opens the way for *in vitro* and *in vivo* testing of synthesized derivatives as potent inhibitors with an improved pharmacological profile against farnesyl diphosphate synthase, phosphodiesterase III, CXCR4, and GABA_A receptor agonists.

■ ASSOCIATED CONTENT

SI Supporting Information

The Supporting Information is available free of charge at <https://pubs.acs.org/doi/10.1021/acsomega.2c01570>.

General experimental section, characterization data, FT-IR, ¹H, and ¹³C NMR spectra for selected synthesized compound, secondary structures of biological targets, docking scores, optimized geometries of some structures (PDF)

■ AUTHOR INFORMATION

Corresponding Author

Pratibha Sharma — School of Chemical Sciences, Devi Ahilya University, Indore 452001 Madhya Pradesh, India;
orcid.org/0000-0002-3106-1100;
Email: drpratibhasharma@yahoo.com

Authors

Deepika Geedkar — School of Chemical Sciences, Devi Ahilya University, Indore 452001 Madhya Pradesh, India
Ashok Kumar — School of Chemical Sciences, Devi Ahilya University, Indore 452001 Madhya Pradesh, India;
orcid.org/0000-0002-9596-3971

Complete contact information is available at:
<https://pubs.acs.org/10.1021/acsomega.2c01570>

Notes

The authors declare no competing financial interest.

■ REFERENCES

- (1) Rotstein, B. H.; Zaretsky, S.; Rai, V.; Yudin, A. K. Small heterocycles in multicomponent reactions. *Chem. Rev.* **2014**, *114*, 8323–8359.
- (2) Deep, A.; Bhatia, R. K.; Kaur, R.; Kumar, S.; Jain, U. K.; Singh, H.; Batra, S.; Kaushik, D.; Deb, P. K. Imidazo[1,2-*a*]pyridine Scaffold as Prospective Therapeutic Agents. *Curr. Top. Med. Chem.* **2016**, *17*, 238–250.
- (3) Tanishima, S.; Morio, Y. A review of minodronic acid hydrate for the treatment of osteoporosis. *Clin Interv Aging.* **2013**, *8*, 185–189.
- (4) Mizushige, K.; Ueda, T.; Yukiiri, K.; Suzuki, H. Olprinone: a phosphodiesterase III inhibitor with positive inotropic and vasodilator effects. *Cardiovasc. Drug Rev.* **2002**, *20*, 163–174.
- (5) Langer, S. Z.; Arbilla, S.; Benavides, J.; Scatton, B. Zolpidem and alpidem: two imidazopyridines with selectivity for omega 1-and omega 3-receptor subtypes. *Adv. Biochem Psychopharmacol* **1990**, *46*, 61–72.
- (6) Almirante, L.; Polo, L.; Mugnaini, A.; Provinciali, E.; Rugarli, P.; Biancotti, A.; Gamba, A.; Murmann, W. Derivatives of Imidazole. I. Synthesis and Reactions of Imidazo[1,2-*a*]pyridines with Analgesic, Antiinflammatory, Antipyretic, and Anticonvulsant Activity. *J. Med. Chem.* **1965**, *8*, 305–312.
- (7) Boerner, R. J.; Moller, H. J. Saripidem—a new treatment for panic disorders. *Psychopharmakother.* **1997**, *4*, 145–148.
- (8) Gudmundsson, K.; Boggs, S. D. PCT Int. Appl, Patent No. WO/2006/026703, 2006.
- (9) John, A.; Shaikh, M. M.; Ghosh, P. Palladium Complexes of Abnormal N-heterocyclic Carbenes as Precatalysts for the Much Preferred Cu-Free and Amine-Free Sonogashira Coupling in Air in a Mixed-aqueous Medium. *Dalton Trans.* **2009**, *47*, 10581–10591.
- (10) Bae, J. S.; Lee, D. W.; Lee, D. H.; Jeong, D. S. PCT Int. Appl, Patent No. WO/2007/011163A1, 2007.
- (11) Bagdi, A. K.; Santra, S.; Monir, K.; Hajra, A. Synthesis of imidazo[1,2-*a*]pyridines: a decade update. *Chem. Commun.* **2015**, *51*, 1555–1575.
- (12) Mohareb, R. M.; Manhi, F. M.; Mahmoud, M. A.; Abdelwahab, A. Uses of dimedone to synthesis pyrazole, isoxazole, and thiophene derivatives with antiproliferative, tyrosine kinase and Pim-1 kinase inhibitions. *Med. Chem. Res.* **2020**, *29*, 1536–1551.
- (13) Gawande, M. B.; Bonifacio, V. D. B.; Luque, R.; Branco, P. S.; Varma, R. S. Benign by Design: Catalyst-Free In-Water, On-Water Green Chemical Methodologies in Organic Synthesis. *Chem. Soc. Rev.* **2013**, *42*, 5522–5551.
- (14) Du, L. H.; Wang, Y. G. A Rapid and Efficient Synthesis of Benzimidazoles Using Hypervalent Iodine as Oxidant. *Synthesis* **2007**, *38*, 675–678.
- (15) Moghaddam, F. M.; Bardajee, G. R.; Ismaili, H.; Taimoory, S. M. D. Facile and Efficient One-Pot Protocol for the Synthesis of Benzoxazole and Benzothiazole Derivatives using Molecular Iodine as Catalyst. *Synth. Commun.* **2006**, *36*, 2543–2548.
- (16) Yang, C. H.; Chen, X.; Li, H.; Wei, W.; Yang, Z.; Chang, J. Iodine Catalyzed Reduction of Quinolines under Mild Reaction Conditions. *Chem. Commun.* **2018**, *54*, 8622–8625.
- (17) Prajapati, D.; Gohain, M. Iodine a Simple, Effective and Inexpensive Catalyst for the Synthesis of Substituted Coumarins. *Catal. Lett.* **2007**, *119*, 59–63.
- (18) Fujioka, H.; Komatsu, H.; Nakamura, T.; Miyoshi, A.; Hata, K.; Ganesh, J.; Murai, K.; Kita, Y. Organic synthesis using a hypervalent iodine reagent: unexpected and novel domino reaction leading to spiro cyclohexadienone lactones. *Chem. Commun.* **2010**, *46*, 4133–4135.
- (19) Ren, Y. M.; Cai, C.; Yang, R. C. Molecular iodine-catalyzed multicomponent reactions: An efficient catalyst for organic synthesis. *RSC Adv.* **2013**, *3*, 7182–7204.
- (20) Wang, X.; Yan, F.; Wang, Q. Molecular iodine: Catalysis in heterocyclic synthesis. *Synth. Commun.* **2021**, *51*, 1763–1781.
- (21) Deghady, A. M.; Hussein, R. K.; Alhamzani, A. G.; Mera, A. Density Functional Theory and Molecular Docking Investigations of

- the Chemical and Antibacterial Activities for 1-(4-Hydroxyphenyl)-3-phenylprop-2-en-1-one. *Molecules* **2021**, *26*, 3631–3643.
- (22) Geedkar, D.; Kumar, A.; Sharma, P. Multiwalled carbon nanotubes crowned with nickel-ferrite magnetic nanoparticles assisted heterogeneous catalytic strategy for the synthesis of benzo[*d*]imidazo[2,1-*b*]thiazole scaffolds. *J. Heterocycl. Chem.* **2020**, *57*, 4331–4347.
- (23) Geedkar, D.; Kumar, A.; Reen, G. K.; Sharma, P. Titania-silica nanoparticles ensembles assisted heterogeneous catalytic strategy for the synthesis of pharmacologically significant 2,3-diaryl-3,4-dihydroimidazo[4,5-*b*]indole scaffolds. *J. Heterocycl. Chem.* **2020**, *57*, 1963–1973.
- (24) Geedkar, D.; Kumar, A.; Kumar, K.; Sharma, P. Hydromagnesite sheets impregnated with cobalt–ferrite magnetic nanoparticles as heterogeneous catalytic system for the synthesis of imidazo[1,2-*a*]pyridine scaffolds. *RSC Adv.* **2021**, *11*, 23207–23220.
- (25) Protein Data Bank [Research Collaboratory for Structural Bioinformatics (RCSB)], <http://www.rcsb.org/pdb/explore/explore.do?structureId=5CGS>, accessed April 2021.
- (26) Protein Data Bank [Research Collaboratory for Structural Bioinformatics (RCSB)], <http://www.rcsb.org/pdb/explore/explore.do?structureId=1SO2>, accessed April 2021.
- (27) Protein Data Bank [Research Collaboratory for Structural Bioinformatics (RCSB)], <http://www.rcsb.org/pdb/explore/explore.do?structureId=4COF>, accessed April 2021.
- (28) Protein Data Bank [Research Collaboratory for Structural Bioinformatics (RCSB)], <http://www.rcsb.org/pdb/explore/explore.do?structureId=3OE0>, accessed April 2021.
- (29) *Molegro Virtual Docker*, version 6.0.0; CLC Bio: Aarhus N, Denmark, 2012.
- (30) Payra, S.; Saha, A.; Wu, C. M.; Selvaratnam, B.; Dramstad, T.; Mahoney, L.; Verma, S. K.; Thareja, S.; Koodali, R.; Banerjee, S. Fe–SBA-15 catalyzed synthesis of 2-alkoxyimidazo [1, 2-*a*] pyridines and screening of their in silico selectivity and binding affinity to biological targets. *New J. Chem.* **2016**, *40*, 9753–9760.
- (31) Verma, S. K.; Thareja, S. Molecular docking assisted 3D-QSAR study of benzylidene-2, 4-thiazolidinedione derivatives as PTP-1B inhibitors for the management of Type-2 diabetes mellitus. *RSC Adv.* **2016**, *6*, 33857–33868.
- (32) *BIOVIA DS, Discovery Visualizer Studio*, v19.1.0.18287; Dassault Systèmes: San Diego, CA, USA, 2019.
- (33) *QSAR, ADMET, and Predictive Toxicology with Biovia Discovery Studio Datasheet Predicting Development Risks*; Dassault Systèmes Corporate: Waltham, MA, USA; BIOVIA Corporate Americas: San Diego, CA, USA; BIOVIA Corporate Europe; Cambridge, UK, 2016; DS No. 3057-1014.
- (34) Frisch, M. J.; Trucks, G. W.; Schlegel, H. B.; Scuseria, G. E.; Robb, M. A.; Cheeseman, J. R.; Scalmani, G.; Barone, V.; Mennucci, B.; Petersson, G. A.; Nakatsuji, H.; Caricato, M.; Li, X.; Hratchian, H. P.; Izmaylov, A. F.; Bloino, J.; Zheng, G.; Sonnenberg, J. L.; Hada, M.; Ehara, M.; Toyota, K.; Fukuda, R.; Hasegawa, J.; Ishida, M.; Nakajima, T.; Honda, Y.; Kitao, O.; Nakai, H.; Vreven, T.; Montgomery, J. A., Jr.; Peralta, J. E.; Ogliaro, F.; Bearpark, M.; Heyd, J. J.; Brothers, E.; Kudin, K. N.; Staroverov, V. N.; Kobayashi, R.; Normand, J.; Raghavachari, K.; Rendell, A.; Burant, J. C.; Iyengar, S. S.; Tomasi, J.; Cossi, M.; Rega, N.; Millam, J. M.; Klene, M.; Knox, J. E.; Cross, J. B.; Bakken, V.; Adamo, C.; Jaramillo, J.; Gomperts, R.; Stratmann, R. E.; Yazyev, O.; Austin, A. J.; Cammi, R.; Pomelli, C.; Ochterski, J. W.; Martin, R. L.; Morokuma, K.; Zakrzewski, V. G.; Voth, G. A.; Salvador, P.; Dannenberg, J. J.; Dapprich, S.; Daniels, A. D.; Farkas, O.; Foresman, J. B.; Ortiz, J. V.; Cioslowski, J.; Fox, D. J. *Gaussian 09*, Revision E.01; Gaussian, Inc.: Wallingford, CT, 2013.
- (35) Mebi, C. A. DFT study on structure, electronic properties, and reactivity of cis-isomers of [(NC₅H₄S)₂Fe(CO)₂]. *J. Chem. Sci.* **2011**, *123*, 727–731.
- (36) Franco-Perez, M.; Gazquez, J. L. Electronegativities of Pauling and Mulliken in Density Functional Theory. *J. Phys. Chem. A* **2019**, *123*, 10065–10071.
- (37) Parr, R. G.; Pearson, R. G. Absolute hardness: companion parameter to absolute electronegativity. *J. Am. Chem. Soc.* **1983**, *105*, 7512–7516.
- (38) Sukumar, N. A. *Matter of Density: Exploring the Electron Density Concept in the Chemical, Biological, and Materials Sciences*; Wiley: Hoboken, NJ, USA, 2012; pp 157–201.
- (39) Parr, R. G.; Yang, W. Density functional approach to the frontier-electron theory of chemical reactivity. *J. Am. Chem. Soc.* **1984**, *106*, 4049–4050.
- (40) Rangel-Galván, M.; Castro, M. E.; Perez-Aguilar, J. M.; Caballero, N. A.; Rangel-Huerta, A.; Melendez, F. J. Theoretical Study of the Structural Stability, Chemical Reactivity, and Protein Interaction for NMP Compounds as Modulators of the Endocannabinoid System. *Molecules* **2022**, *27*, 414–429.
- (41) Karamthulla, S.; Khan, M. N.; Choudhury, L. H. Microwave-assisted synthesis of novel 2,3-disubstituted imidazo[1,2-*a*]pyridines via one-pot three-component reactions. *RSC Adv.* **2015**, *5*, 19724–19733.
- (42) Brahmachari, G.; Nayek, N.; Karmakar, I.; Nurjamil, K.; Chandra, S. K.; Bhowmick, A. Series of Functionalized 5-(2-Arylimidazo[1,2-*a*]pyridin-3-yl)pyrimidine-2,4(1H,3H)-diones: A Water-Mediated Three-Component Catalyst-Free Protocol Revisited. *J. Org. Chem.* **2020**, *85*, 8405–8414.
- (43) Zhang, G.; Guo, S.; Cui, H.; Qi, J. Virtual Screening of Small Molecular Inhibitors against DprE1. *Molecules* **2018**, *23*, 524–532.
- (44) Tanwar, G.; Mazumder, A. G.; Bhardwaj, V.; Kumari, S.; Bharti, R.; Yamini, Singh, D.; Das, P.; Purohit, R. Target identification, screening and in vivo evaluation of pyrrolone-fused benzosuberene compounds against human epilepsy using Zebrafish model of pentylentetrazol-induced seizures. *Sci. Rep.* **2019**, *9*, 1–12.
- (45) Lipinski, C. A. Lead and drug-like compounds: the rule-of-five revolution. *Drug Discov Today Technol.* **2004**, *1*, 337–341.
- (46) Mendoza-Huizar, L. H.; Rios Reyes, C. H. Chemical Reactivity of Atrazine Employing the Fukui Function. *J. Mex. Chem. Soc.* **2011**, *55*, 142–147.
- (47) Piyanzina, I.; Minisini, B.; Tayurskii, D.; Bardeau, J. F. Density functional theory calculations on azobenzene derivatives: a comparative study of functional group effect. *J. Mol. Model.* **2015**, *21*, 34–38.
- (48) Ghanty, T. K.; Ghosh, S. K. A Density Functional Approach to Hardness, Polarizability, and Valency of Molecules in Chemical Reactions. *J. Phys. Chem.* **1996**, *100*, 12295–12298.
- (49) Senet, P. Chemical hardnesses of atoms and molecules from frontier orbitals. *Chem. Phys. Lett.* **1997**, *275*, 527–532.
- (50) Parr, R. G.; Von-Szentpaly, L.; Liu, S. Electrophilicity Index. *J. Am. Chem. Soc.* **1999**, *121*, 1922–1924.
- (51) Pearson, R. G. Chemical hardness and density functional theory. *J. Chem. Sci.* **2005**, *117*, 369–377.
- (52) Mottishaw, J. D.; Erck, A. R.; Kramer, J. H.; Sun, H.; Koppang, M. Electrostatic Potential Maps and Natural Bond Orbital Analysis: Visualization and Conceptualization of Reactivity in Sanger's Reagent. *J. Chem. Educ.* **2015**, *92*, 1846–1852.
- (53) Ahmed, A.; Fatima, A.; Shakyia, S.; Rahman, Q. I.; Ahmad, M.; Javed, S.; AlSalem, H. S.; Ahmad, A. Crystal Structure, Topology, DFT and Hirshfeld Surface Analysis of a Novel Charge Transfer Complex (L3) of Anthraquinone and 4-[(anthracen-9-yl)methyl]amino}-benzoic Acid (L2) Exhibiting Photocatalytic Properties: An Experimental and Theoretical Approach. *Molecules* **2022**, *27*, 1724–1745.